COMPUTER VISION, GRAPHICS, AND IMAGE PROCESSING 26, 73–106 (1984)

New Likelihood Test Methods for Change Detection in Image Sequences

Y. Z. HSU,* H.-H. NAGEL,† AND G. REKERS

Fachbereich Informatik, Universitaet Hamburg, Schlueterstrasse 70, D-2000 Hamburg 13, West Germany

Received November 17, 1982

Modeling the image as a piecewise linear gray-value function of the pixel coordinates considerably improved a change detection test based previously on a piecewise constant gray-value function. These results encouraged investigations into modeling the picture as a mosaic of patches where the gray-value function within each patch is described as a second-order bivariate polynomial of the pixel coordinates. Such a more appropriate model allowed the assumption to be made that the remaining gray-value variation within each patch can be attributed to noise related to the sensing and digitizing devices, independent of the individual image frames in a sequence. This assumption made it possible to relate the likelihood test for change detection to well-known statistical tests (t test, F test), facilitating the determination of threshold values related to a priori confidence limits.

1. INTRODUCTION

Image sequences offer the possibility of sensing, storing, and analyzing information about dynamic developments in a scene. A recent book by Huang [7] provides a convenient introduction to this area.

An algorithmic analysis of digital image sequences attempts to interpret changes between consecutive image frames. An important starting point for such interpretation attempts is the hypothesis that observable interframe differences should be attributed to relative motion between the image sensor and objects in the scene. Various approaches toward this goal as well as the relations among them have been discussed in a recent condensed survey by Nagel [15]. Here, we will concentrate on the subproblem of how to detect and combine interframe differences as a kind of preprocessing for more involved interpretation algorithms.

The next section delineates the subproblem to be discussed here and outlines a technique previously used. The third section describes an improved technique based on a more appropriate model of the picture function. Various results obtained by this approach are shown.

These results encouraged investigations of modeling the picture function as consisting of patches within which the gray values vary as a second-order bivariate polynomial in the pixel coordinates. The improvements resulting from this extension will be discussed in Section 4.

This model of the local gray-value distribution appears to capture the significant structural variation. As a consequence, it is assumed that any remaining variation can be attributed to noise related to the sensing and digitizing devices. The

*On leave of absence from Shanghai Institute for Computer Technology, Shanghai, People's Republic of China.

†Present address: Fraunhofer-Institut für Informations- und Datenverarbeitung IITB, Sebastian-Kneipp-Strasse 12-14, 7500 Karlsruhe 1, West Germany.

0734-189X/84 $3.00

remaining variation should, therefore, be independent of the individual image content. Once this assumption appears justified, it becomes possible to derive the probability distribution for the likelihood ratio by relating it to those encountered in well-known statistical tests. This will be developed for a constant picture function in Section 5, for a linear picture function in Section 6, and for a quadratic picture function in Section 7. Results will be discussed in Section 8.

2. DETECTION OF CHANGES

A good TV camera with a signal-to-noise ratio in excess of about 45 db warrants quantization of the gray-value signal into 256 gray levels (8-bit representation). If the gray levels obtained at the same image coordinates in two consecutive frames differ by more than two or three levels, such a change is usually considered to be significant, e.g., in the context of interframe coding for bandwidth compression. Difficulties may be encountered in textured areas with high spatial frequency components or in slowly displaced subimages with low contrast. If the threshold for gray-value differences is too high, significant changes might be suppressed, whereas too low a threshold overcrowds the difference image with noise. This dilemma becomes especially important if the signal-to-noise ratio is reduced, for example, due to real-time buffering on an analog video disk or tape.

Since noise is assumed to be spatially uncorrelated, one may discriminate a significant change area by postulating a minimum number of spatially adjacent pixels with interframe gray-value differences above the threshold. Alternatively, one may check the compatibility of gray-value distributions from entire test areas rather than by comparing the gray values of individual pixels. A likelihood test originally developed by Yakimovsky for the segmentation of gray-value images [23, 13] has been adapted for interframe compatibility tests [14].

Yakimovsky designed the test in order to decide between two hypotheses, namely, that the gray values observed in two spatially adjacent test areas are compatible (H_0) or not (H_1) [23]. He assumed that the gray values have been drawn independently from one out of three normal distributions: one for the left or upper test area 1, one for the right or lower test area 2, or one normal distribution common to the joint area 0. The mean μ and variance σ^2 characterizing each of these three normal distributions are determined from the gray values observed in the respective test area, based on the maximum likelihood estimate. If both test areas 1 and 2 comprise the same number n of pixels, the likelihood ratio derived by Yakimovsky [23] may be written in the form

$$\frac{\text{likelihood}(H_1)}{\text{likelihood}(H_0)} = \frac{\sigma_0^{2n}}{\sigma_1^n \sigma_2^n} \tag{1}$$

or

$$\left[\frac{\text{likelihood}(H_1)}{\text{likelihood}(H_0)}\right]^{2/n} = \frac{\left[(\sigma_1^2 + \sigma_2^2)/2 + ((\mu_1 - \mu_2)/2)^2\right]^2}{\sigma_1^2 \sigma_2^2}. \tag{2}$$

Exponentiation by $2/n$ has been used in order to avoid unnecessary computations. The numerator on the right-hand side of Eq. (2) represents the squared variance of the combined area 0, using mean values and variances for the two constituent test areas 1 and 2. If this expression exceeds a threshold T we decide in favor of hypothesis H_1, i.e. the two test areas have incompatible gray-value distributions. Therefore, an edge element has to be placed between these two spatially adjacent test areas. If, however, the expression of equation (2) is less or equal to the threshold T, the observed gray values are considered to be drawn from a single normal distribution, i.e. we decide in favor of hypothesis H_0 that the gray-value distributions in the two test areas are compatible. In this case, no edge element will be placed between the two spatially adjacent test areas.

Nagel instead used test areas comprising the same pixel locations, but in different frames [14]. A decision in favor of hypothesis 1 implied incompatible gray-value distributions at these test areas from different frames, i.e. a temporal change. This approach has been employed in other investigations at our laboratory [9, 10].

Figure 1 shows three consecutive frames (BILD10, BILD11, BILD12) from a street scene sequence recorded in real time by a TV camera on an analog video disk. Each frame has been subsequently digitized into 574 lines of 512 pixels with 8-bit gray values. The mean and variance were estimated for a test area comprising four consecutive pixels in three consecutive lines from the first half-frame of each TV image. Such a test area corresponds to a square on the image sensor. One half-frame is therefore represented by an array of 96 lines each of which comprises 128 consecutive test areas.

a

FIG. 1. Facsimile writer output of digitized data from three consecutive frames of a street scene image sequence recorded at 40-msec time intervals: (a) BILD10, (b) BILD11, (c) BILD12.

b

c

FIG. 1.—*Continued*

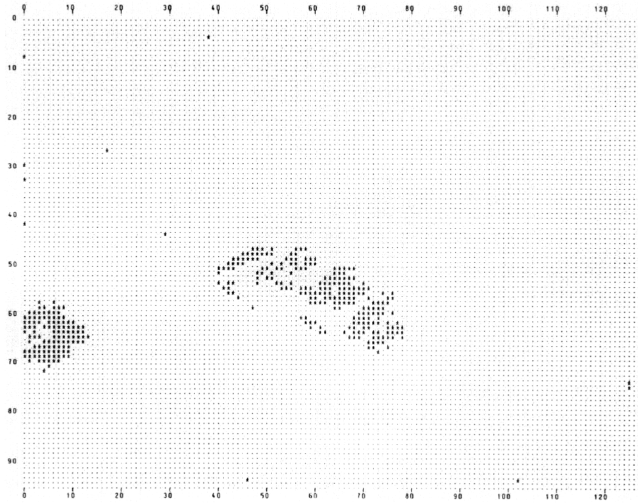

FIG. 2. A binary image of 96 lines with 128 columns each, representing the test areas used for the interframe comparison between frames BILD10 and BILD11 (see Fig. 1). An asterisk marks the position of test areas with incompatible gray-value distributions according to Eq. (2), based on a threshold $T = 4$.

Figure 2 shows a binary image where each asterisk indicates that the gray-value distributions of frames BILD10 and BILD11 were incompatible in the corresponding test areas, based on a threshold value of $T = 4$.

Figure 3 gives the corresponding results for the interframe comparison between BILD11 and BILD12. Apart from isolated changes, indications for three moving objects can be recognized: the bright taxicab in the center, a dark car entering the field of view from the left, and a van just entering from the right.

The important point to note is the fact that despite a heavy clustering of changes, for example, around the bright taxicab, the incompatible test areas nevertheless

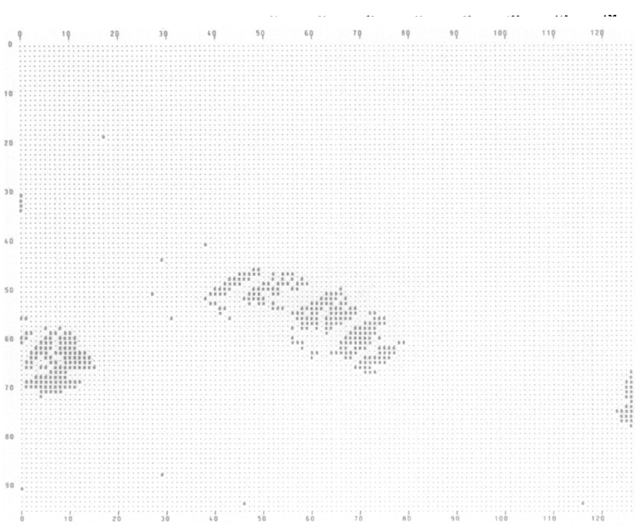

FIG. 3. Analogous to Fig. 2, but comparing BILD11 with BILD12.

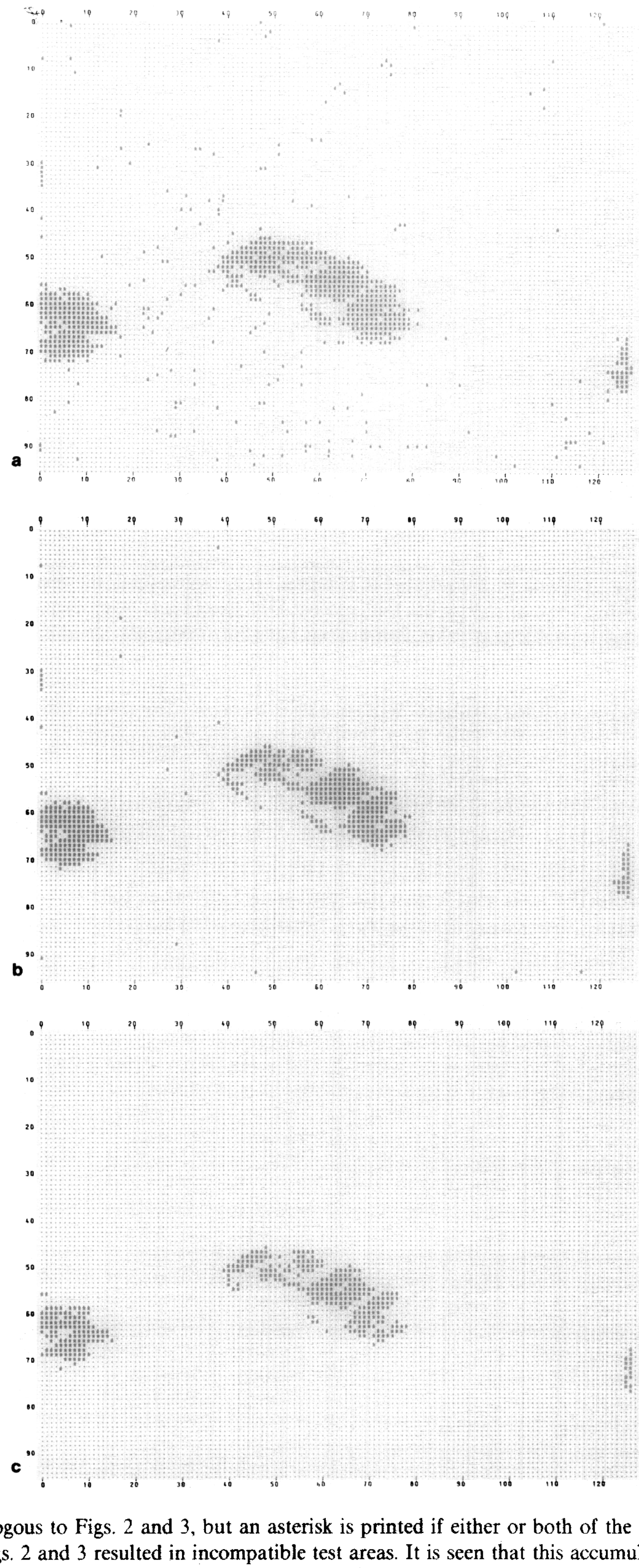

FIG. 4. Analogous to Figs. 2 and 3, but an asterisk is printed if either or both of the interframe pairs presented in Figs. 2 and 3 resulted in incompatible test areas. It is seen that this accumulation of change indicators yields a mask for a substantial part of the moving object although more or less homogeneous regions are still not covered. Results are given for three different threshold values: (a) $T = 2.5$, (b) $T = 4.0$, (c) $T = 10.0$.

cannot be simply joined by requiring four-connection or eight-connection. This becomes even more obvious if the threshold is raised from 2.5 to 4 or 10 in order to suppress change indications due to noise. This problem has been circumvented currently by comparing a series of consecutive frames with a reference frame, usually the first one, using additive combination of change indications [9, 10]; see, for example, Fig. 4.

Such an approach can only be employed if the accumulated change indications are caused by the same object. This will not be the case, for example, if the distance between two moving objects is so small that their change areas merge before sufficiently complete masks for the individual object images could have been generated. Moreover, the mask derived in this manner will cover considerable area belonging to the background if it is applied to extract an image of the moving object from any particular frame contributing to its generation.

Various means have been studied to employ such accumulated masks in order to extract an object image [8, 9, 11].

An even more sensitive but nevertheless robust test appears to be desirable. The following section describes a refinement of the likelihood test considered so far, resulting in a rather robust technique.

3. PIECEWISE LINEAR GRAY-VALUE VARIATIONS AS A MODEL FOR THE PICTURE FUNCTION

Equation (2) has been derived based on the assumption that the gray-value distribution within a test area is adequately described by a normal distribution centered on a constant mean gray value. Any deviations from the mean gray value have to be attributed to noise. This is equivalent to assuming that the image can be adequately modeled as a mosaic of areas each of which has a constant gray value and some area-specific variance.

In general, such a model of the picture function is inadequate. A somewhat better approximation allows at least for a linear slope of gray values with the pixel coordinates in the area. Approaches in this direction have recently been reviewed by Haralick [4], who did not mention, however, the work by Holdermann and Kazmierczak [6] or by Radig [20, 21]; see also Haralick and Watson [5] as well as Pong *et al.* [19]. Yakimovsky, too, generalized the likelihood ratio according to Eq. (2) for the situation of a linearly sloping gray-value distribution [23]:

$$\left[\frac{\text{likelihood}\,(H_1)}{\text{likelihood}\,(H_0)}\right]^{2/n} = \frac{\left(\sigma_0^2\right)^2}{\sigma_1^2\sigma_2^2} \tag{3}$$

with

$$\sigma_i^2 = (1/n) \sum_{x,\,y\in A_i} \left[\beta_{i1} + \beta_{i2}x + \beta_{i3}y - g(x, y)\right]^2 \tag{4}$$

where $g(x, y)$ denotes the gray value at pixel location (x, y) within the test area A_i. Here, $\beta_{i1} + \beta_{i2}x + \beta_{i3}y$ describes the linear gray-value function with coefficients obtained by a least-squares error fit to the gray values measured within the test area A_i. Since a linearly sloping gray-value distribution will be approximated by a more adequate image model, the variance σ_i^2 will be smaller. This should facilitate a

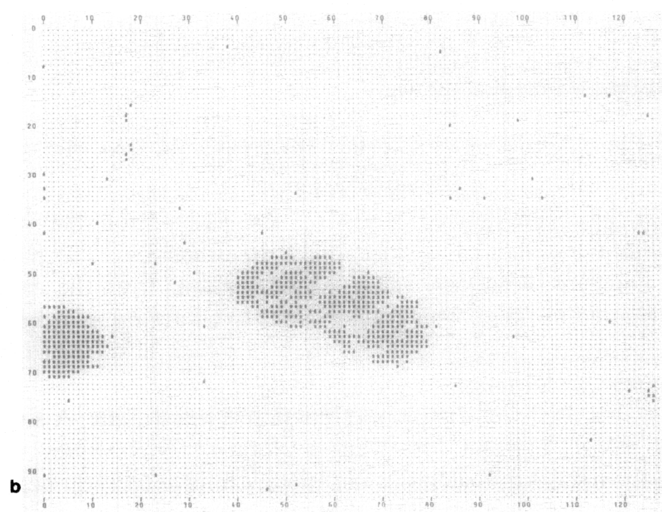

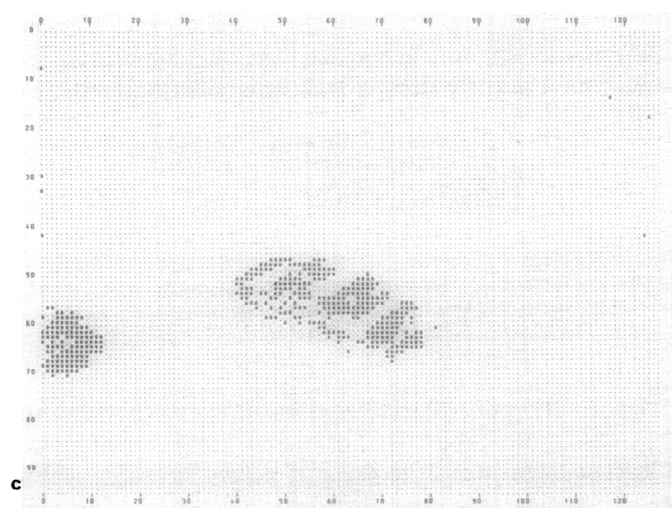

FIG. 5. Analogous to Fig. 2, but using a linearly sloping picture function model rather than a constant one as in Fig. 2. Note that the changed test areas cover the taxicab in the center of the image frame much more completely. Thresholds T used for the expression of Eq. (3) based on Eq. (4) are (a) $T = 2.5$, (b) $T = 4.0$, (c) $T = 10.0$.

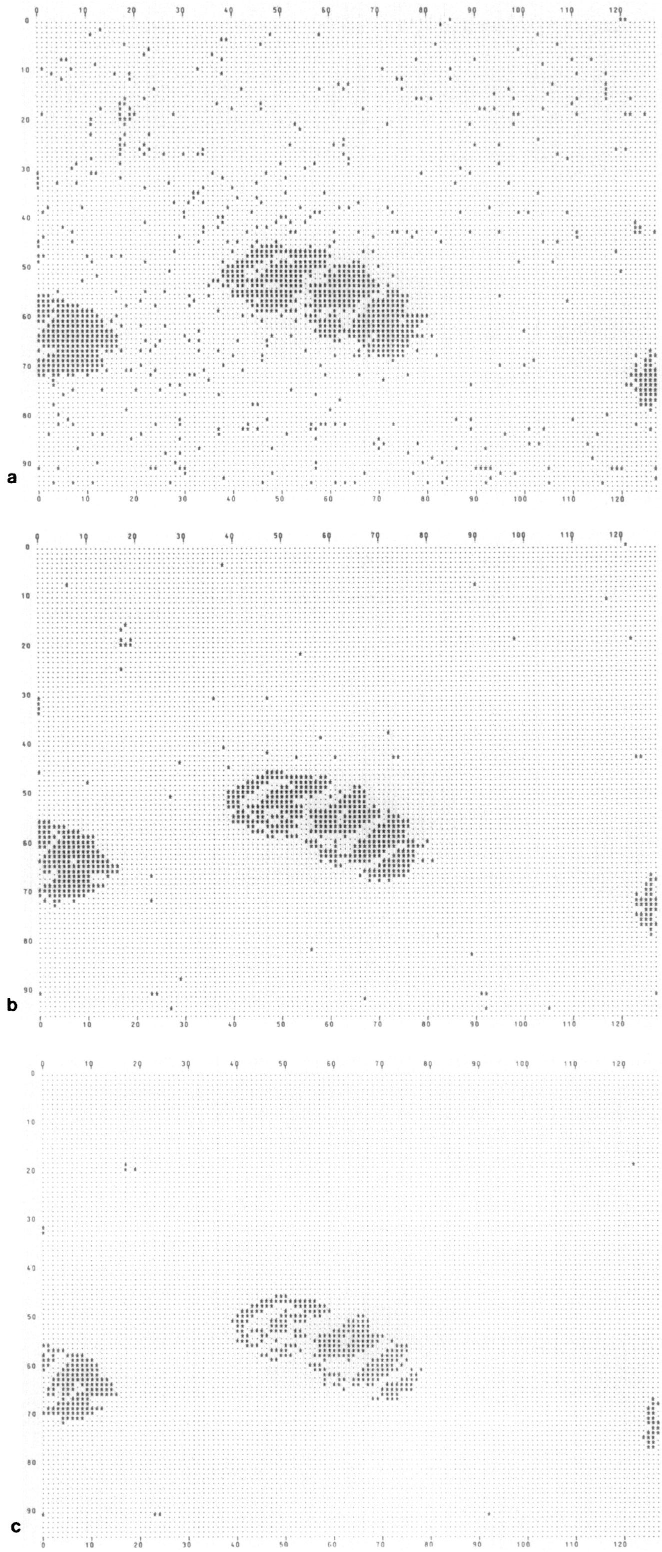

FIG. 6. Analogous to Fig. 5, but comparing BILD11 with BILD12; see Fig. 3 to notice the difference between constant and linearly sloping picture functions within a test area. (a) $T = 2.5$, (b) $T = 4.0$, (c) $T = 10.0$.

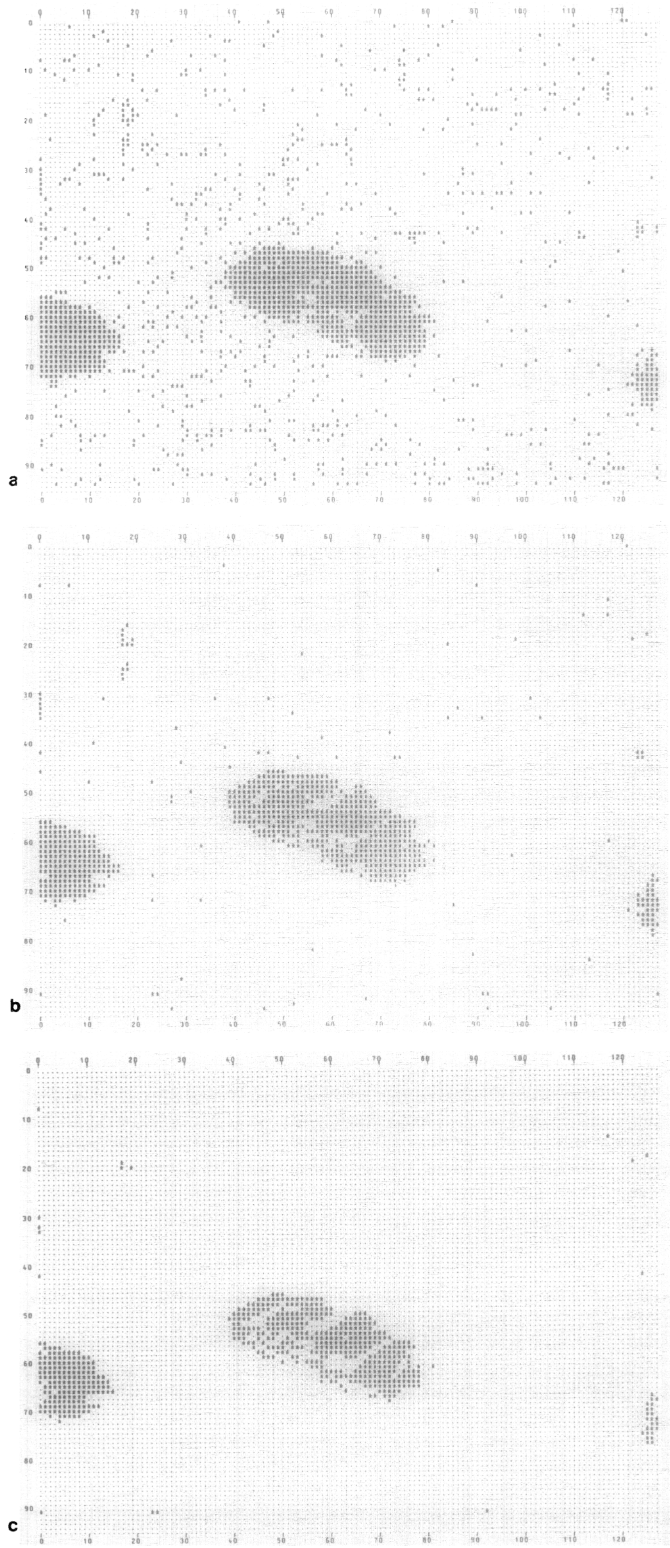

FIG. 7. Analogous to Fig. 4, i.e., the accumulated changes between BILD10 and BILD11 as well as between BILD11 and BILD12, but for a linearly sloping picture function: (a) $T = 2.5$, (b) $T = 4.0$, (c) $T = 10.0$.

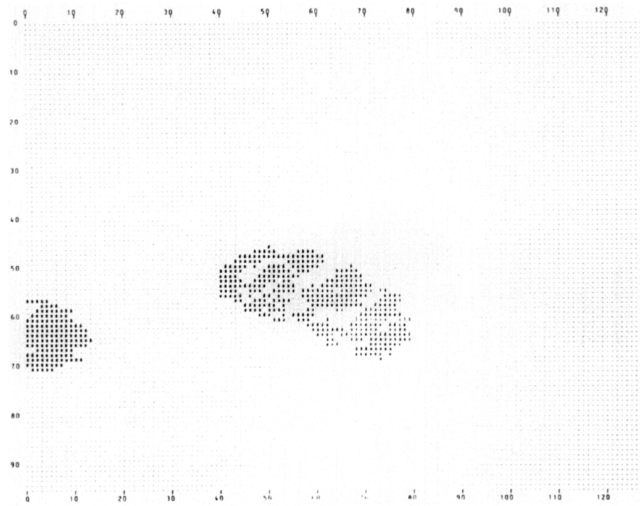

FIG. 8. Like Fig. 5b, but with suppression of isolated changes.

distinction between a systematic gray-value slope and large gray-value fluctuations caused, for example, by high spatial frequency texture.

In analogy to the approach reported in the preceding section [14] we investigated Eqs. (3) and (4) in order to test the compatibility of gray-value distributions from test areas at the same position in two different frames. Initial experiments were hampered by the absence of suitable visualization aids and gave inconclusive results [12]. Once a raster display had become available, however, experimental problems could be studied in more detail. Due to the vagaries of random sampling it may happen that the estimated variance is much smaller than the true variance—possibly even zero. In order to avoid unreasonable results, the estimated variances are replaced by a standard value of 1.0 whenever they turn out to be smaller.

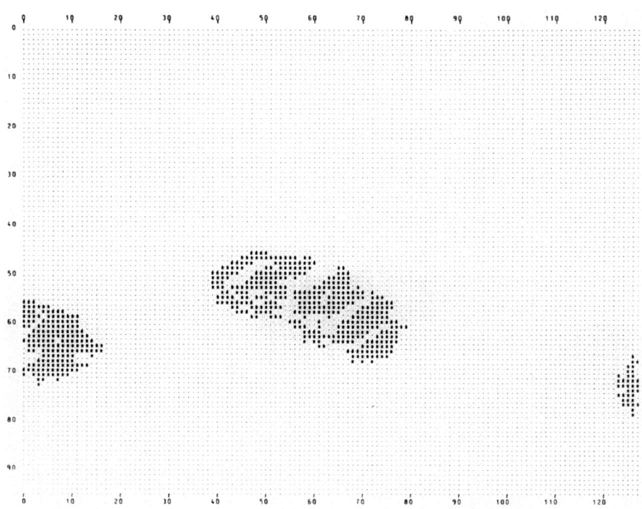

FIG. 9. Like Fig. 6b, but with suppression of isolated changes.

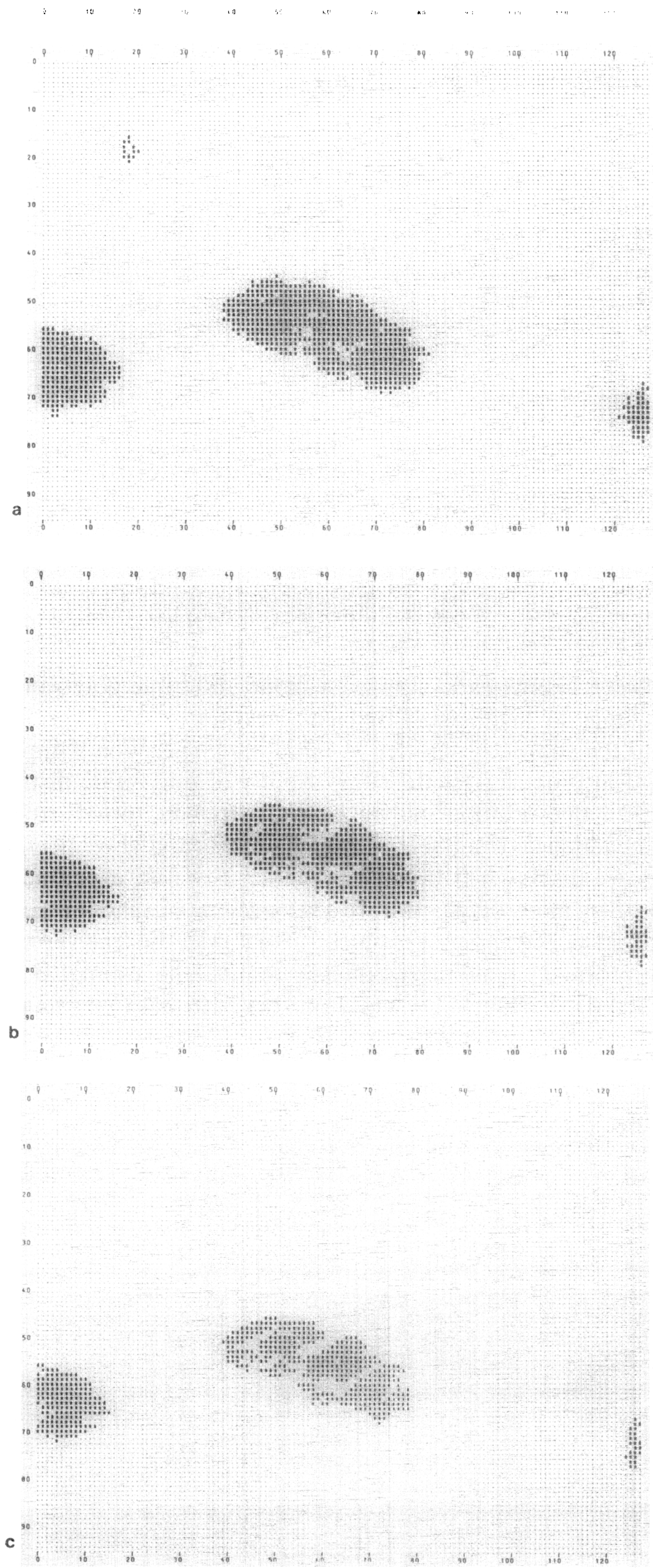

FIG. 10. Like Fig. 7, but with suppression of isolated changes, i.e., disjunctive combination of Figs. 8 and 9, representing changes between BILD11 and the preceding BILD10 as well as the subsequent BILD12. The remaining changes around line 20 in Fig. 10a (T = 2.5) have been caused by a walking pedestrian who changes his/her location only very little between three frames, i.e., in less than one-tenth of a second. Therefore, these changes are not so strong and disappear at higher thresholds of T = 4 (Fig. 10b) or T = 10.0 (Fig. 10c).

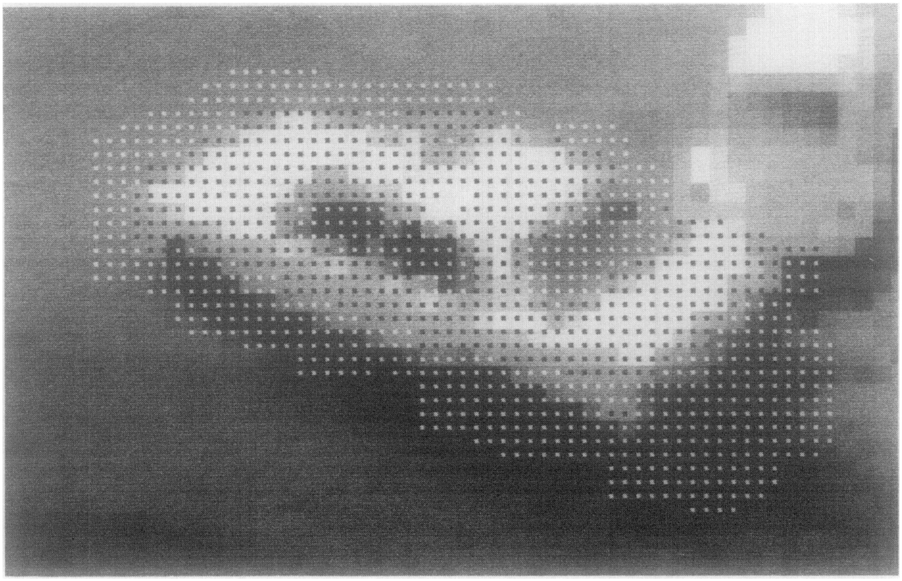

FIG. 11. Mask for the taxicab, obtained by interactive selection of this change region from Fig. 10b and subsequent expansion by 1 pixel. The result is overlayed on the second frame (b) from Fig. 1.

Figures 5 through 7 represent the analog to Figs. 2 through 4, but for a linearly sloping picture function rather than the constant one previously used. One easily recognizes that the test has become more sensitive. Already the accumulation of changes from two successive interframe comparisons represents a fairly complete mask of the moving object in this example. Isolated noise changes have increased, too. They are, however, easily suppressed by the requirement that only regions with more than N ($= 10$) four-connected changed test areas are retained; see Figs. 8 through 11 [18].

4. EXPERIMENTAL INVESTIGATIONS WITH PIECEWISE QUADRATIC PICTURE FUNCTIONS

The results reported in the preceding section warranted closer investigation. It turned out that for images with much detail like those of Fig. 1, a linear picture function is not sufficient to model the actual gray-value distribution within the image subareas employed here, namely three consecutive rows with four pixels each from one half-frame [22]. As a consequence, the variance estimated according to Eq. (4) is biased by contributions from gray-value transition areas inadequately described by a linear picture function.

We repeated the experiments using a quadratic picture function to model the gray-value distribution within each test area, i.e., replacing Eq. (4) by

$$\sigma_i^2 = \frac{1}{n} \sum_{x,\, y \in A_i} \left[\beta_{i1} + \beta_{i2}x + \beta_{i3}y + \beta_{i4}x^2 + \beta_{i5}y^2 + \beta_{i6}xy - g(x, y)\right]^2. \quad (5)$$

Figure 12 shows which test areas changed in this case from BILD10 to BILD11 and Fig. 13 is analogous for BILD11 and BILD12. Figure 14 presents the disjunctive

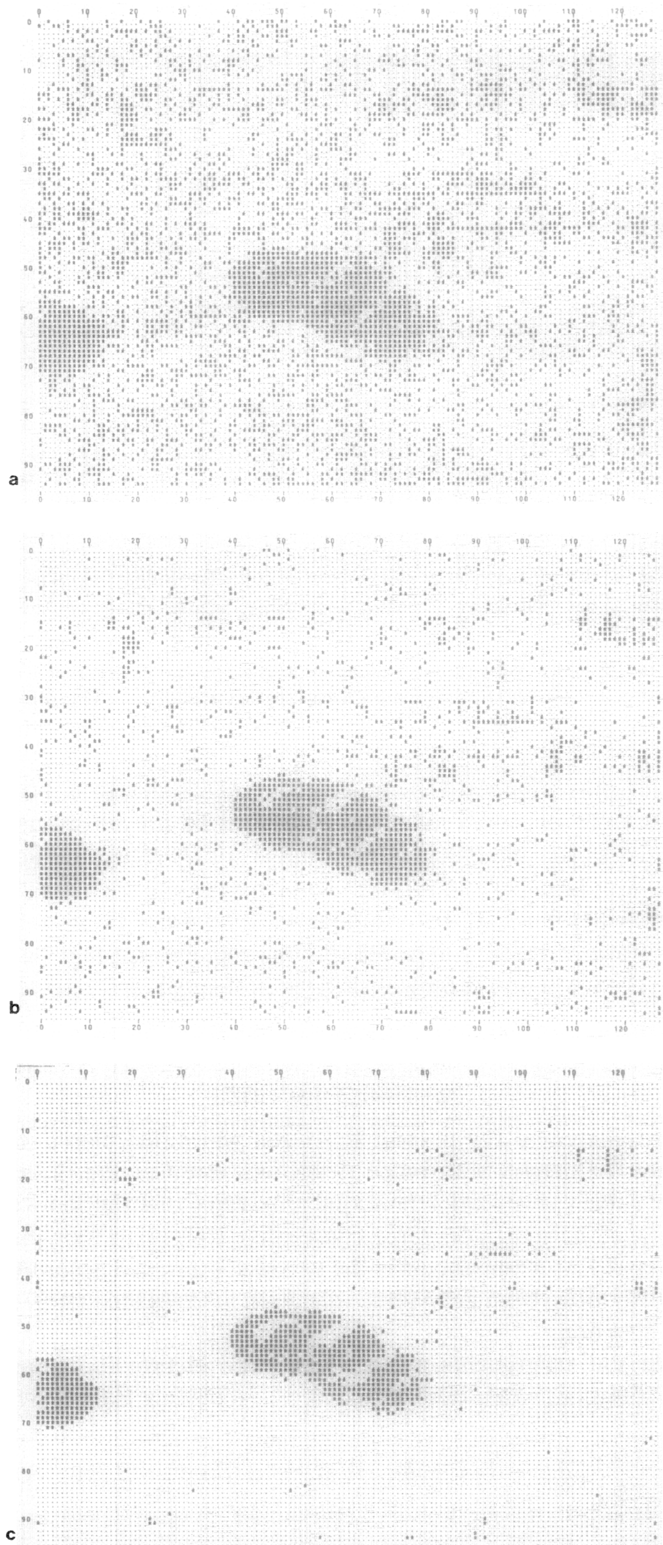

FIG. 12. Analogous to Figs. 2 and 5, but using the quadratic picture function (5): (a) $T = 2.5$, (b) $T = 4.0$, (c) $T = 10.0$.

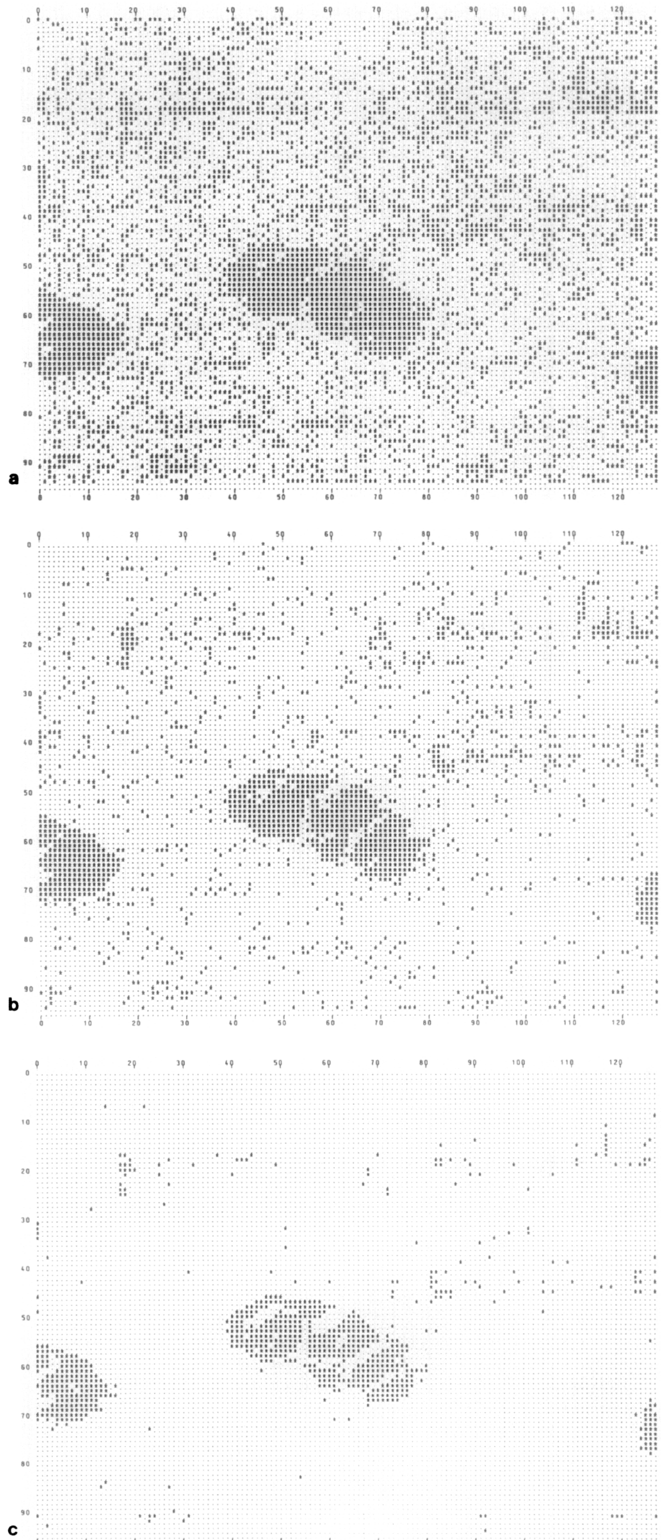

FIG. 13. Analogous to Fig. 12, but comparing BILD11 with BILD12; see also Figs. 3 and 6. (a) $T = 2.5$, (b) $T = 4.0$, (c) $T = 10.0$.

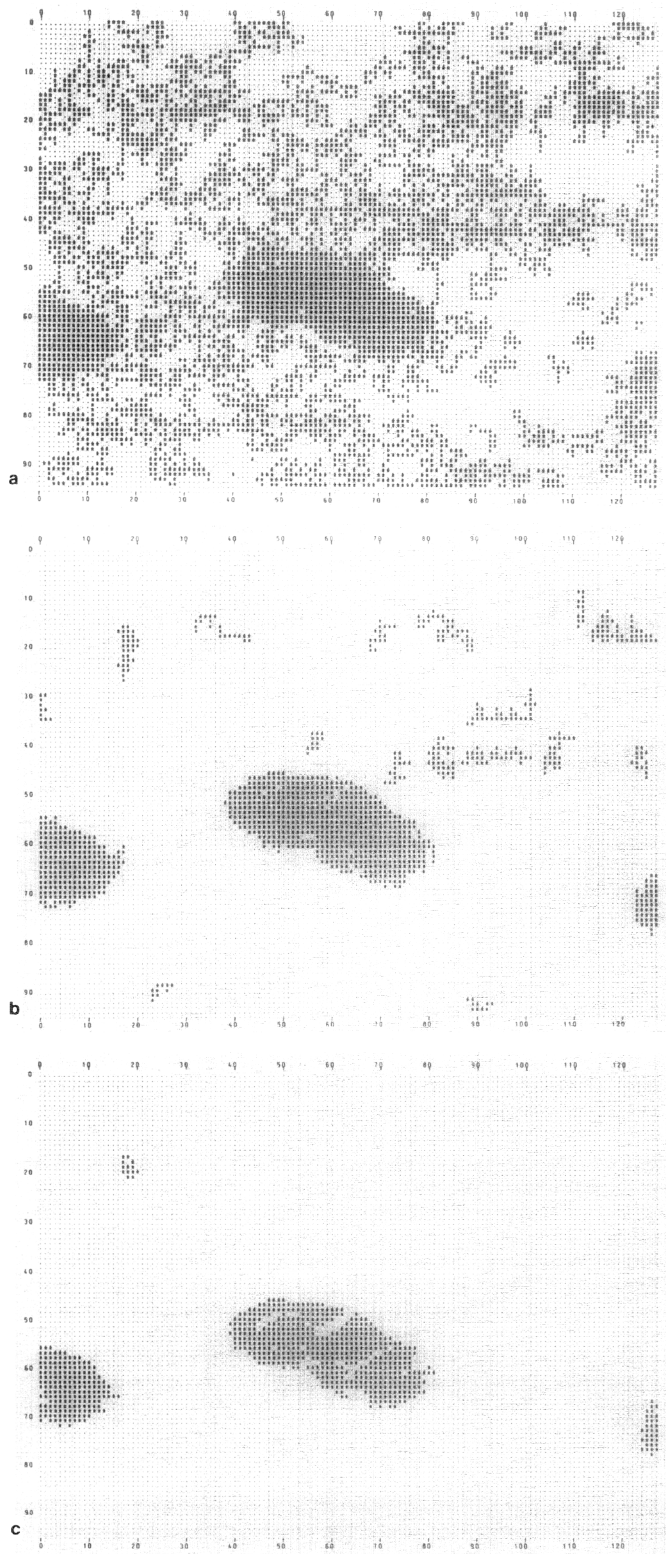

FIG. 14. Disjunctive combination of changes from BILD11 to the preceding frame as well as to the subsequent one using the quadratic picture function to model the gray-value distribution within each test area with suppression of isolated changes; compare Fig. 10: (a) $T = 2.5$, (b) $T = 4.0$, (c) $T = 10.0$.

combination of changes from BILD11 to the preceding one as well as to the subsequent one with suppression of isolated changes. In all experiments reported so far, the threshold T to be compared to the expression obtained from Eq. (3) combined with Eq. (4) or (5) has been chosen interactively. Although the exact value appeared to be uncritical for various image sequences, in principle it has to be adjusted for each sequence. Moreover, such a procedure does not allow us to quantify the confidence level at which the decisions about change versus no change are made.

Nevertheless, these experiments support the hypothesis that a quadratic picture function model captures enough of the systematic gray-value variation within each test area to yield a reliable change detection result. Parallel investigations aiming at the determination of interframe displacement vectors in [1–3, 16, 17] provide additional evidence that the gray-value distribution in local test areas can be adequately approximated by a second-order bivariate polynomial of the two image plane coordinates.

A consequence of accepting this hypothesis is the assumption that the variance determined according to Eq. (5) no longer comprises contributions by inadequately modeled gray-value structures. It should be entirely due to noise. We assume that the measured gray values are corrupted by additive noise due to the digitizing hardware. It therefore appears reasonable to consider the noise in measurements from both test areas to be compared as being identically distributed provided we record the TV frame series under constant conditions. Under this assumption we derive the probability distribution of the maximum likelihood ratio for piecewise constant, piecewise linear, and piecewise quadratic gray-value variations. In these situations we can employ the t test (for constant) or the F test (for linear and quadratic variations) as a change detection test. We therefore arrive at a common algorithm which can be used without interactive threshold adjustment by selecting an adequate threshold according to some a priori confidence limit.

5. THRESHOLD SELECTION FOR A PIECEWISE CONSTANT PICTURE FUNCTION

Let $g_i^{(1)}$ $(i = 1, \ldots, m)$, $g_j^{(2)}$ $(j = 1, \ldots, n)$ be observed values from the two test areas N_1, N_2, respectively. They correspond to gray values corrupted by normally distributed noise with mean 0 and variance σ^2. The joint probability distribution for the observation of these measurements in the case of n sample values is given by the likelihood function

$$L = f(g, \mu, \sigma) = \left(\frac{1}{2\pi\sigma^2}\right)^{n/2} \exp\left\{-\frac{1}{2\sigma^2}\sum_{i=1}^{n}(g_i - \mu)^2\right\} \tag{6}$$

where μ represents the mean of the distribution of sample values.

The hypothesis to be tested now is denoted by:

H_0: $g^{(1)}$ and $g^{(2)}$ come from the same distribution $N(\mu_0, \sigma_0)$.

H_1: $g^{(1)}$ and $g^{(2)}$ come from different distributions $N(\mu_1, \sigma)$ and $N(\mu_2, \sigma)$.

The optimal estimators for mean and variance maximize the likelihood function. The resulting expressions for these estimators differ according to which hypothesis is selected.

When H_1 is true, the maximum likelihood function will be

$$L(H_1) = \left(\frac{1}{2\pi\sigma^2}\right)^{(m+n)/2} \exp\left\{-\frac{1}{2\sigma^2}\left[\sum_{i=1}^{m}\left(g_i^{(1)} - \mu_1\right)^2 + \sum_{j=1}^{n}\left(g_j^{(2)} - \mu_2\right)^2\right]\right\}. \quad (7)$$

Calculating the partial derivatives with respect to σ^2, μ_1, μ_2 and equating them to zero yield

$$\hat{\mu}_1 = \frac{1}{m}\sum_{i=1}^{m} g_i^{(1)} \quad (8a)$$

$$\hat{\mu}_2 = \frac{1}{n}\sum_{j=1}^{n} g_j^{(2)} \quad (8b)$$

$$\hat{\sigma}^2 = \hat{\sigma}_1^2 = \hat{\sigma}_2^2 = \frac{1}{m+n}\left[\sum_{i=1}^{m}\left(g_i^{(1)} - \hat{\mu}_1\right)^2 + \sum_{j=1}^{n}\left(g_j^{(2)} - \hat{\mu}_2\right)^2\right]. \quad (8c)$$

When H_0 is true, then

$$\hat{\mu}_0 = \frac{1}{m+n}\left[\sum_{i=1}^{m} g_i^{(1)} + \sum_{j=1}^{n} g_j^{(2)}\right] = \frac{1}{m+n}\left(m\hat{\mu}_1 + n\hat{\mu}_2\right) \quad (9a)$$

and

$$\begin{aligned}\hat{\sigma}_0^2 &= \frac{1}{m+n}\left[\sum_{i=1}^{m}\left(g_i^{(1)} - \hat{\mu}_0\right)^2 + \sum_{j=1}^{n}\left(g_j^{(2)} - \hat{\mu}_0\right)^2\right] \\ &= \frac{1}{m+n}\left[\sum_{i=1}^{m}\left(g_i^{(1)} - \hat{\mu}_1\right)^2 + \sum_{j=1}^{n}\left(g_j^{(2)} - \hat{\mu}_2\right)^2 + \frac{mn}{m+n}\left(\hat{\mu}_1 - \hat{\mu}_2\right)^2\right]. \quad (9b)\end{aligned}$$

If we use these estimates, the maximum likelihood ratio can be written in the form

$$\begin{aligned}\lambda &= \frac{L(H_1)}{L(H_0)} \\ &= \frac{\left[\dfrac{m+n}{2\pi\left[\sum_{i=1}^{m}\left(g_i^{(1)} - \hat{\mu}_1\right)^2 + \sum_{j=1}^{n}\left(g_j^{(2)} - \hat{\mu}_2\right)^2\right]}\right]^{(m+n)/2} * \exp\left\{-\dfrac{m+n}{2}\right\}}{\left[\dfrac{m+n}{2\pi\left[\sum_{i=1}^{m}\left(g_i^{(1)} - \hat{\mu}_1\right)^2 + \sum_{j=1}^{n}\left(g_j^{(2)} - \hat{\mu}_2\right)^2 + (mn/(m+n))(\hat{\mu}_1 - \hat{\mu}_2)^2\right]}\right]^{(m+n)/2} * \exp\left\{-\dfrac{m+n}{2}\right\}} \\ &= \left[1 + \frac{(mn/(m+n))(\hat{\mu}_1 - \hat{\mu}_2)^2}{\sum_{i=1}^{m}\left(g_i^{(1)} - \hat{\mu}_1\right)^2 + \sum_{j=1}^{n}\left(g_j^{(2)} - \hat{\mu}_2\right)^2}\right]^{(m+n)/2} \quad (10)\end{aligned}$$

We know that $\hat{\mu}_1$ and $\hat{\mu}_2$ possess independent normal distributions $N(\mu_1, \sigma^2/m)$ and $N(\mu_2, \sigma^2/n)$, respectively, and $u = \hat{\mu}_1 - \hat{\mu}_2$ is a normal variable with mean $\mu_1 - \mu_2$ and variance $\sigma^2(1/m + 1/n)$. Under the assumption H_0 the variable u has mean 0, i.e.,

$$w = \frac{\hat{\mu}_1 - \hat{\mu}_2}{\sigma(1/m + 1/n)^{1/2}} \tag{11}$$

is a normal variable with mean 0 and variance 1. If H_0 is true, then $\Sigma_{i=1}^{m}(g_i^{(1)} - \hat{\mu}_1)^2/\sigma^2$ and $\Sigma_{j=1}^{n}(g_j^{(2)} - \hat{\mu}_2)^2/\sigma^2$ possess independent χ^2 distributions with $m - 1$ and $n - 1$ degrees of freedom, respectively. Hence their sum $V = \Sigma_{i=1}^{m}(g_i^{(1)} - \hat{\mu}_1)^2/\sigma^2 + \Sigma_{j=1}^{n}(g_j^{(2)} - \hat{\mu}_2)/\sigma^2$ is a χ^2 variable with $m + n - 2$ degrees of freedom.

Then the variable

$$\begin{aligned} t &= \frac{w}{(V/(m+n-2))^{1/2}} \\ &= \frac{(mn/(m+n))^{1/2}(\hat{\mu}_1 - \hat{\mu}_2)}{\left[\sum_{i=1}^{m}\left(g_i^{(1)} - \hat{\mu}_1\right)^2/(m+n-2) + \sum_{j=1}^{n}\left(g_j^{(2)} - \hat{\mu}_2\right)^2/(m+n-2)\right]^{1/2}} \end{aligned} \tag{12}$$

obeys the student t distribution with $m + n - 2$ degrees of freedom provided H_0 is true. The maximum likelihood ratio now is

$$\lambda = \left[1 + \frac{t^2}{m+n-2}\right]^{(m+n)/2}. \tag{13}$$

As λ is a monotonic function of t^2, we can test t^2 instead of λ. We can select a threshold t_α according to a confidence α. For example, if $m = n = 12$, for confidence $\alpha = 5\%$, then $t_{0.05} = 1.717$ and $t_{0.05}^2 = 2.948$; for confidence $\alpha = 1\%$, one obtains $t_{0.01} = 2.508$ and $t_{0.01}^2 = 6.29$. When the value of t^2 is less than t_α^2, choose hypothesis H_0. Otherwise, H_1 will be accepted.

6. THRESHOLD SELECTION FOR A PIECEWISE LINEAR PICTURE FUNCTION

Let $g_i^{(k)}$ $(k = 1,2;\ i = 1,\ldots,n)$ be n gray values observed in two test areas from two adjacent frames, and let

$$g_i^{(k)} = \beta_{k1} + \beta_{k2}x_i + \beta_{k3}y_i + e_i \qquad (k = 1,2;\ i = 1,\ldots,n) \tag{14}$$

where e_i $(i = 1,\ldots,n)$ are normal noise variables with mean 0 and covariance $I\sigma^2$; $x_i^{(1)} = x_i^{(2)}$, $y_i^{(1)} = y_i^{(2)}$ $(i = 1,\ldots,n)$ are two sets of observed coordinates in both test windows.

The maximum likelihood function here is

$$L = f(g, \beta, \sigma) = \left(\frac{1}{2\pi\sigma^2}\right)^{n/2} \exp\left\{-\frac{\sum_{i=1}^{n}(g_i - \beta_1 - \beta_2 x_i - \beta_3 y_i)^2}{2\sigma^2}\right\}. \tag{15}$$

The hypothesis to be tested is similar to that for a piecewise constant picture function:

H_0: $g^{(1)}$ and $g^{(2)}$ come from the same distribution with parameters β_{01}, β_{02}, β_{03}, and σ_0^2.

H_1: $g^{(1)}$ and $g^{(2)}$ come from distributions with different parameters β_{k1}, β_{k2}, β_{k3} $(k = 1, 2)$, and σ_1^2.

When H_1 is true, the maximum likelihood function will be

$$L = \left(\frac{1}{2\pi\sigma^2}\right)^{n/2} \times \exp\left\{-\frac{\sum_{i=1}^{n}\left(g_i^{(1)} - \beta_{11} - \beta_{12}x_i - \beta_{13}y_i\right)^2 + \sum_{j=1}^{n}\left(g_j^{(2)} - \beta_{21} - \beta_{22}x_j - \beta_{23}y_j\right)^2}{2\sigma^2}\right\}. \tag{16}$$

The optimal estimators for the parameters under the hypothesis H_1 are

$$\hat\beta_{k1} = \frac{1}{n}\sum_{i=1}^{n} g_i^{(k)} \tag{17a}$$

$$\hat\beta_{k2} = \frac{\sum_{i=1}^{n} x_i g_i^{(k)}}{\sum_{i=1}^{n} x_i^2} \tag{17b}$$

$$\hat\beta_{k3} = \frac{\sum_{i=1}^{n} y_i g_i^{(k)}}{\sum_{i=1}^{n} y_i^2} \tag{17c}$$

$$\hat\sigma_1^2 = \frac{1}{2n}\left[\sum_{i=1}^{n}\left(g_i^{(1)} - \hat\beta_{11} - \hat\beta_{12}x_i - \hat\beta_{13}y_i\right)^2 + \sum_{j=1}^{n}\left(g_j^{(2)} - \hat\beta_{21} - \hat\beta_{22}x_j - \hat\beta_{23}y_j\right)^2\right]. \tag{17d}$$

If H_0 is true, then

$$\hat\beta_{01} = \frac{1}{2n}\left[\sum_{i=1}^{n} g_i^{(1)} + \sum_{j=1}^{n} g_j^{(2)}\right] = \tfrac{1}{2}[\hat\beta_{11} + \hat\beta_{21}] \tag{18}$$

$$\hat\beta_{02} = \frac{\sum_{i=1}^{2n} x_i g_i}{\sum_{i=1}^{2n} x_i^2} = \frac{\sum_{i=1}^{n} x_i g_i^{(1)} + \sum_{j=1}^{n} x_j g_j^{(2)}}{2\sum_{i=1}^{n} x_i^2} = \tfrac{1}{2}[\hat\beta_{12} + \hat\beta_{22}] \tag{19}$$

$$\hat{\beta}_{03} = \frac{\sum_{i=1}^{2n} y_i g_i}{\sum_{i=1}^{2n} y_i^2} = \frac{\sum_{i=1}^{n} y_i g_i^{(1)} + \sum_{j=1}^{n} y_j g_j^{(2)}}{2\sum_{i=1}^{n} y_i^2} = \tfrac{1}{2}[\hat{\beta}_{13} + \hat{\beta}_{23}] \tag{20}$$

$$\begin{aligned}
\hat{\sigma}_0^2 &= \frac{1}{2n}\sum_{i=1}^{2n}(g_i - \hat{\beta}_{01} - \hat{\beta}_{02}x_i - \hat{\beta}_{03}y_i)^2 \\
&= \frac{1}{2n}\Bigg[\sum_{i=1}^{n}\left(g_i^{(1)} - \hat{\beta}_{01} - \hat{\beta}_{02}x_i - \hat{\beta}_{03}y_i\right)^2 \\
&\qquad + \sum_{j=1}^{n}\left(g_j^{(2)} - \hat{\beta}_{01} - \hat{\beta}_{02}x_j - \hat{\beta}_{03}y_j\right)^2\Bigg] \\
&= \frac{1}{2n}\Bigg[\sum_{i=1}^{n}\Big\{g_i^{(1)} - \hat{\beta}_{11} - \hat{\beta}_{12}x_i - \hat{\beta}_{13}y_i + \tfrac{1}{2}(\hat{\beta}_{11} - \hat{\beta}_{21}) \\
&\qquad + \tfrac{1}{2}(\hat{\beta}_{12} - \hat{\beta}_{22})x_i + \tfrac{1}{2}(\hat{\beta}_{13} - \hat{\beta}_{23})y_i\Big\}^2 \\
&\qquad + \sum_{j=1}^{n}\Big\{g_j^{(2)} - \hat{\beta}_{21} - \hat{\beta}_{22}x_j - \hat{\beta}_{23}y_j \\
&\qquad + \tfrac{1}{2}(\hat{\beta}_{21} - \hat{\beta}_{11}) + \tfrac{1}{2}(\hat{\beta}_{22} - \hat{\beta}_{12})x_j + \tfrac{1}{2}(\hat{\beta}_{23} - \hat{\beta}_{13})y_j\Big\}^2\Bigg] \\
&= \frac{1}{2n}\Bigg[\sum_{i=1}^{n}\left(g_i^{(1)} - \hat{\beta}_{11} - \hat{\beta}_{12}x_i - \hat{\beta}_{13}y_i\right)^2 \\
&\qquad + \sum_{j=1}^{n}\left(g_j^{(2)} - \hat{\beta}_{21} - \hat{\beta}_{22}x_j - \hat{\beta}_{23}y_j\right)^2 \\
&\qquad + \tfrac{1}{2}\sum_{j=1}^{n}\left\{\hat{\beta}_{11} - \hat{\beta}_{21} + (\hat{\beta}_{12} - \hat{\beta}_{22})x_j + (\hat{\beta}_{13} - \hat{\beta}_{23})y_j\right\}^2\Bigg].
\end{aligned} \tag{21}$$

If we center the coordinate system within the test area and select x_i, y_i $(i = 1,\dots,n)$ so that the sums satisfy

$$\sum_{i=1}^{n} x_i = \sum_{i=1}^{n} y_i = \sum_{i=1}^{n} x_i y_i = 0 \tag{22}$$

then (21) becomes

$$\hat{\sigma}_0^2 = \hat{\sigma}_1^2 + \frac{1}{2n}\left\{\frac{n}{2}(\hat{\beta}_{11} - \hat{\beta}_{21})^2 + \tfrac{1}{2}(\hat{\beta}_{12} - \hat{\beta}_{22})^2\sum_{i=1}^{n} x_i^2 + \tfrac{1}{2}(\hat{\beta}_{13} - \hat{\beta}_{23})^2\sum_{i=1}^{n} y_i^2\right\}. \tag{23}$$

The maximum likelihood ratio is now

$$\lambda = \left[1 + \frac{\frac{1}{2}\left[n(\hat{\beta}_{11} - \hat{\beta}_{21})^2 + (\hat{\beta}_{12} - \hat{\beta}_{22})^2 \sum_{i=1}^{n} x_i^2 + (\hat{\beta}_{13} - \hat{\beta}_{23})^2 \sum_{i=1}^{n} y_i^2 \right]}{\sum_{i=1}^{n} \left(g_i^{(1)} - \hat{\beta}_{11} - \hat{\beta}_{12} x_i - \hat{\beta}_{13} y_i \right)^2 + \sum_{j=1}^{n} \left(g_j^{(2)} - \hat{\beta}_{21} - \hat{\beta}_{22} x_j - \hat{\beta}_{23} y_j \right)^2} \right]^{n}. \tag{24}$$

It can be easily proven that all the following variables are normally distributed with zero mean and unit variance provided H_0 is true:

$$\frac{\hat{\beta}_{11} - \hat{\beta}_{21}}{\sigma[2/n]^{1/2}} \tag{25a}$$

$$\frac{\hat{\beta}_{12} - \hat{\beta}_{22}}{\sigma\left[2/\sum_{i=1}^{n} x_i^2\right]^{1/2}} \tag{25b}$$

$$\frac{\hat{\beta}_{13} - \hat{\beta}_{23}}{\sigma\left[2/\sum_{i=1}^{n} y_i^2\right]^{1/2}}. \tag{25c}$$

It follows from (25) that the variable

$$F_1 = \frac{1}{2\sigma^2}\left\{ n(\hat{\beta}_{11} - \hat{\beta}_{21})^2 + (\hat{\beta}_{12} - \hat{\beta}_{22})^2 \sum_{i=1}^{n} x_i^2 + (\hat{\beta}_{13} - \hat{\beta}_{23})^2 \sum_{i=1}^{n} y_i^2 \right\} \tag{26}$$

possesses a χ^2 distribution with 3 degrees of freedom. The variable

$$F_2 = \frac{\sum_{i=1}^{n} \left(g_i^{(1)} - \hat{\beta}_{11} - \hat{\beta}_{12} x_i - \hat{\beta}_{13} y_i \right)^2 + \sum_{j=1}^{n} \left(g_j^{(2)} - \hat{\beta}_{21} - \hat{\beta}_{22} x_j - \hat{\beta}_{23} y_j \right)^2}{\sigma^2} \tag{27}$$

is a χ^2 variable with $n - 3 + n - 3 = 2n - 6$ degrees of freedom. The maximum likelihood ratio—provided H_0 is true—is given by

$$\lambda = \left[1 + \frac{3}{2n-6} \frac{F_1/3}{F_2/(2n-6)} \right]^n = \left[1 + \frac{3}{2n-6} F \right]^n \tag{28}$$

where $F = (F_1/3)/(F_2/(2n-6))$ is an F variable with 3 and $2n - 6$ degrees of freedom.

If $n = 12$ and the confidence limit is taken as $\alpha = 5\%$, then $F_{0.05} = 3.16$. If the confidence limit $\alpha = 1\%$ is selected, then $F_{0.01} = 5.09$. Since λ is a monotonic function of F, we can accept H_0 when $F < F_\alpha$ and choose H_1 when $F > F_\alpha$. This procedure for change detection between frames is analogous to the one described in [4] for edge detection within one frame.

7. THRESHOLD SELECTION FOR A PIECEWISE QUADRATIC PICTURE FUNCTION

It is assumed that

$$G = X\beta + e \tag{29}$$

where G is a set of uncorrelated observed gray values; β is an unknown 6-dimensional parameter vector; e is an uncorrelated n-normal variable vector with mean 0 and covariance $I\sigma^2$; X is a $n \times 6$ matrix, and every row vector $x_i = (x_{i1}, x_{i2}, \ldots, x_{i6})$ denotes a set of observed coordinate functions. These functions are $x_{i1} = 1$, $x_{i2} = x_i$, $x_{i3} = y_i$, $x_{i4} = x_i^2$, $x_{i5} = y_i^2$, $x_{i6} = x_i y_i$. The formula (29) can be written as follows:

$$\begin{bmatrix} g_1 \\ g_2 \\ \vdots \\ g_n \end{bmatrix} = \begin{bmatrix} 1 & x_{12} & x_{13} & \cdots & x_{16} \\ 1 & x_{22} & x_{23} & \cdots & x_{26} \\ \vdots & \vdots & \vdots & & \vdots \\ 1 & x_{n2} & x_{n3} & \cdots & x_{n6} \end{bmatrix} * \begin{bmatrix} \beta_1 \\ \beta_2 \\ \vdots \\ \beta_6 \end{bmatrix} + \begin{bmatrix} e_1 \\ e_2 \\ \vdots \\ e_n \end{bmatrix}. \tag{30}$$

Let $G^{(1)}, G^{(2)}$ be observed gray values from two test windows:

$$G^{(1)} = \begin{bmatrix} g^{(1)} \\ g_2^{(1)} \\ \vdots \\ g_n^{(1)} \end{bmatrix}, \qquad G^{(2)} = \begin{bmatrix} g_1^{(2)} \\ g_2^{(2)} \\ \vdots \\ g_n^{(2)} \end{bmatrix}. \tag{31}$$

The hypothesis to be tested is denoted by

H_0: $G^{(1)}$ and $G^{(2)}$ come from the same gray-value distribution $N(\beta, I\sigma)$.

H_1: $G^{(1)}$ and $G^{(2)}$ come from different gray-value distributions $N(\beta^{(1)}, I\sigma)$ and $N(\beta^{(2)}, I\sigma)$.

The likelihood function is now

$$L = f(e, \beta, \sigma) = \left(\frac{1}{2\pi\sigma^2}\right)^{n/2} \exp\left\{-(G - X\beta)^T(G - X\beta)/2\sigma^2\right\}. \tag{32}$$

Using the logarithm, calculating the partial derivatives with respect to σ^2 and β_i, and equating them to 0 will yield the normal equations

$$\log L = -\frac{n}{2}\log(2\pi) - \frac{n}{2}\log\sigma^2 - \frac{1}{2\sigma^2}\left[(G - X\beta)^T(G - X\beta)\right] \tag{33a}$$

$$\frac{\partial \log L}{\partial \beta} = -\frac{1}{2\sigma^2}X^T(G - X\beta) = 0 \tag{33b}$$

$$\frac{\partial \log L}{\partial \sigma^2} = -\frac{n}{2}\frac{1}{\sigma^2} + \frac{1}{2\sigma^4}\left[(G - X\beta)^T(G - X\beta)\right] = 0. \tag{33c}$$

From these we obtain the optimal estimators of β and σ^2

$$\hat{\beta} = (X^T X)^{-1} X^T G \tag{34}$$

$$\hat{\sigma}^2 = \frac{1}{n}\left[(G - X\hat{\beta})^T (G - X\hat{\beta})\right]. \tag{35}$$

When H_1 is true, then

$$\hat{\beta}_1 = (X^T X)^{-1} X^T G^{(1)} \tag{36a}$$

and

$$\hat{\beta}_2 = (X^T X)^{-1} X^T G^{(2)} \tag{36b}$$

$$\hat{\sigma}_1^2 = \frac{1}{2n}\left\{(G^{(1)} - X\hat{\beta}_1)^T (G^{(1)} - X\hat{\beta}_1) + (G^{(2)} - X\hat{\beta}_2)^T (G^{(2)} - X\hat{\beta}_2)\right\}. \tag{37}$$

When H_0 is true, then

$$\hat{\beta}_0 = (X_0^T X_0)^{-1} X_0^T G \tag{38}$$

$$\hat{\sigma}_0^2 = \frac{1}{2n}(G - X_0\hat{\beta}_0)^T (G - X_0\hat{\beta}_0) \tag{39}$$

where

$$X_0 = \begin{bmatrix} X \\ X \end{bmatrix}, \qquad G = \begin{bmatrix} G^{(1)} \\ G^{(2)} \end{bmatrix}. \tag{40}$$

From (40) we have

$$X_0^T = [X^T X^T];$$

$$X_0^T X_0 = [X^T X^T]\begin{bmatrix} X \\ X \end{bmatrix} = X^T X + X^T X = 2X^T X. \tag{41}$$

Hence

$$\begin{aligned} \hat{\beta}_0 &= (X_0^T X_0)^{-1} X_0^T G \\ &= \tfrac{1}{2}(X^T X)^{-1}(X^T G^{(1)} + X^T G^{(2)}) \\ &= \tfrac{1}{2}(\hat{\beta}_1 + \hat{\beta}_2). \end{aligned} \tag{42}$$

Using (40) and (41), Eq. (39) can be written in the form

$$\begin{aligned} \hat{\sigma}_0^2 &= \frac{1}{2n}\begin{bmatrix} G^{(1)} - \frac{1}{2}X(\hat{\beta}_1 + \hat{\beta}_2) \\ G^{(2)} - \frac{1}{2}X(\hat{\beta}_1 + \hat{\beta}_2) \end{bmatrix}^T \begin{bmatrix} G^{(1)} - \frac{1}{2}X(\hat{\beta}_1 + \hat{\beta}_2) \\ G^{(2)} - \frac{1}{2}X(\hat{\beta}_1 + \hat{\beta}_2) \end{bmatrix} \\ &= \frac{1}{2n}\begin{bmatrix} G^{(1)} - X\hat{\beta}_1 + \frac{1}{2}X(\hat{\beta}_1 - \hat{\beta}_2) \\ G^{(2)} - X\hat{\beta}_2 + \frac{1}{2}X(\hat{\beta}_2 - \hat{\beta}_1) \end{bmatrix}^T \begin{bmatrix} G^{(1)} - X\hat{\beta}_1 + \frac{1}{2}X(\hat{\beta}_1 - \hat{\beta}_2) \\ G^{(2)} - X\hat{\beta}_2 + \frac{1}{2}X(\hat{\beta}_2 - \hat{\beta}_1) \end{bmatrix} \\ &= \frac{1}{2n}\left\{\left[G^{(1)} - X\hat{\beta}_1 + \tfrac{1}{2}X(\hat{\beta}_1 - \hat{\beta}_2)\right]^T \left[G^{(1)} - X\hat{\beta}_1 + \tfrac{1}{2}X(\hat{\beta}_1 - \hat{\beta}_2)\right]\right. \\ &\qquad \left. + \left[G^{(2)} - X\hat{\beta}_2 + \tfrac{1}{2}X(\hat{\beta}_2 - \hat{\beta}_1)\right]^T \left[G^{(2)} - X\hat{\beta}_2 + \tfrac{1}{2}X(\hat{\beta}_2 - \hat{\beta}_1)\right]\right\}. \end{aligned} \tag{43}$$

Execution of the matrix multiplications in Eq. (43) will result in terms containing

$$\left(G^{(k)} - X\hat{\beta}_k\right)^T X = \left[X^T\left(G^{(k)} - X\hat{\beta}_k\right)\right]^T = 0 \qquad \text{for } k = 1, 2 \tag{44}$$

which vanish due to Eq. (33b).

Using (44), (43) can be written directly as

$$\begin{aligned}\hat{\sigma}_0^2 &= \frac{1}{2n}\Big\{\left(G^{(1)} - X\hat{\beta}_1\right)^T\left(G^{(1)} - X\hat{\beta}_1\right) + \tfrac{1}{4}(\hat{\beta}_1 - \hat{\beta}_2)^T X^T X(\hat{\beta}_1 - \hat{\beta}_2) \\ &\qquad + \left(G^{(2)} - X\hat{\beta}_2\right)^T\left(G^{(2)} - X\hat{\beta}_2\right) + \tfrac{1}{4}(\hat{\beta}_2 - \hat{\beta}_1)^T X^T X(\hat{\beta}_2 - \hat{\beta}_1)\Big\} \\ &= \hat{\sigma}_1^2 + \frac{1}{4n}(\hat{\beta}_1 - \hat{\beta}_2)^T X^T X(\hat{\beta}_1 - \hat{\beta}_2).\end{aligned} \tag{45}$$

The maximum likelihood ratio λ can therefore be written

$$\lambda = \left[1 + \frac{\frac{1}{2}(\hat{\beta}_1 - \hat{\beta}_2)^T X^T X(\hat{\beta}_1 - \hat{\beta}_2)}{\left(G^{(1)} - X\hat{\beta}_1\right)^T\left(G^{(1)} - X\hat{\beta}_1\right) + \left(G^{(2)} - X\hat{\beta}_2\right)^T\left(G^{(2)} - X\hat{\beta}_2\right)}\right]^n. \tag{46}$$

It is obvious that $\hat{\beta}_k$ are normally distributed according to $N(\beta, \sigma^2(X^TX)^{-1})$ $(k = 1, 2)$ and $\hat{\beta}_1 - \hat{\beta}_2$ are also normal $N(0, 2\sigma^2(X^TX)^{-1})$ when H_0 is true. Therefore

$$F_1 = \frac{\frac{1}{2}(\hat{\beta}_1 - \hat{\beta}_2)^T X^T X(\hat{\beta}_1 - \hat{\beta}_2)}{\sigma^2} \tag{47}$$

is a χ^2 variable with 6 degrees of freedom, and

$$F_2 = \frac{\left(G^{(1)} - X\hat{\beta}_1\right)^T\left(G^{(1)} - X\hat{\beta}_1\right) + \left(G^{(2)} - X\hat{\beta}_2\right)^T\left(G^{(2)} - X\hat{\beta}_2\right)}{\sigma^2} \tag{48}$$

follows a χ^2 distribution with $2n - 12$ degrees of freedom. Finally, the maximum likelihood ratio now is (with $n = 12$ as in our experimental situation)

$$\lambda = \left[1 + \frac{1}{2}\frac{F_1/6}{F_2/12}\right]^n = \left[1 + \frac{1}{2}F\right]^n \tag{49}$$

where

$$F = \frac{F_1/6}{F_2/12} = \frac{(\hat{\beta}_1 - \hat{\beta}_2)^T X^T X(\hat{\beta}_1 - \hat{\beta}_2)}{\left(G^{(1)} - X\hat{\beta}_1\right)^T\left(G^{(1)} - X\hat{\beta}_1\right) + \left(G^{(2)} - X\hat{\beta}_2\right)^T\left(G^{(2)} - X\hat{\beta}_2\right)}. \tag{50}$$

is an F-variable with degrees of freedom $(6, 12)$ when H_0 is true. We can restrict ourselves to test F because λ is a monotonic function of F. If we choose a confidence level α, hypothesis H_1 should be accepted if $F > F_\alpha$. Otherwise H_0 should be accepted.

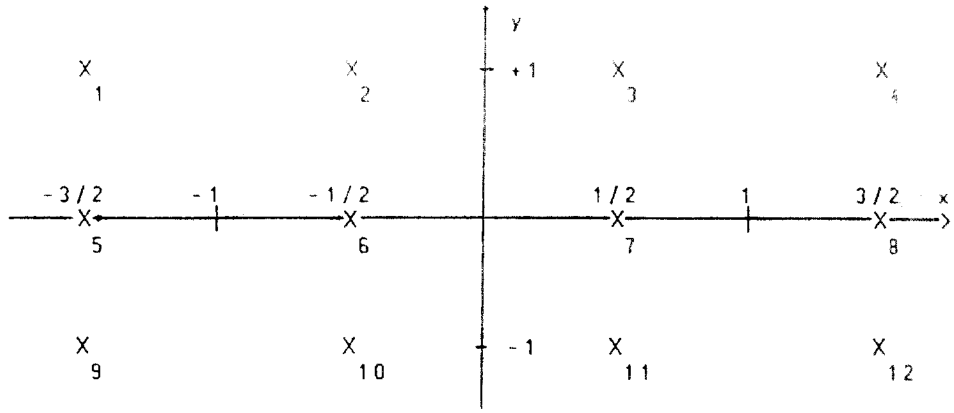

FIG. 15. Positions of sample values in the local test area made up of four consecutive pixels in three consecutive rows from one digitized half-frame.

8. RESULTS AND DISCUSSION

The interframe compatibility tests derived in the preceding sections have been applied to the sequence of three frames depicted in Fig. 1. The coordinates of sample values in each test area are indicated in Fig. 15.

The transpose of the matrix X in Eq. (29) is then given by

$$X^T = \begin{bmatrix} 1 & 1 & 1 & 1 & 1 & 1 & 1 & 1 & 1 & 1 & 1 & 1 \\ -\frac{3}{2} & -\frac{1}{2} & \frac{1}{2} & \frac{3}{2} & -\frac{3}{2} & -\frac{1}{2} & \frac{1}{2} & \frac{3}{2} & -\frac{3}{2} & -\frac{1}{2} & \frac{1}{2} & \frac{3}{2} \\ 1 & 1 & 1 & 1 & 0 & 0 & 0 & 0 & -1 & -1 & -1 & -1 \\ \frac{9}{4} & \frac{1}{4} & \frac{1}{4} & \frac{9}{4} & \frac{9}{4} & \frac{1}{4} & \frac{1}{4} & \frac{9}{4} & \frac{9}{4} & \frac{1}{4} & \frac{1}{4} & \frac{9}{4} \\ 1 & 1 & 1 & 1 & 0 & 0 & 0 & 0 & 1 & 1 & 1 & 1 \\ -\frac{3}{2} & -\frac{1}{2} & \frac{1}{2} & \frac{3}{2} & 0 & 0 & 0 & 0 & \frac{3}{2} & \frac{1}{2} & -\frac{1}{2} & -\frac{3}{2} \end{bmatrix} \tag{51}$$

from which it follows that

$$(X^TX)^{-1}X^T =$$

$$\begin{bmatrix} -\frac{5}{48} & \frac{5}{48} & \frac{5}{48} & -\frac{5}{48} & \frac{7}{48} & \frac{17}{48} & \frac{17}{48} & \frac{7}{48} & -\frac{5}{48} & \frac{5}{48} & \frac{5}{48} & -\frac{5}{48} \\ -\frac{1}{10} & -\frac{1}{30} & \frac{1}{30} & \frac{1}{10} & -\frac{1}{10} & -\frac{1}{30} & \frac{1}{30} & \frac{1}{10} & -\frac{1}{10} & -\frac{1}{30} & \frac{1}{30} & \frac{1}{10} \\ \frac{1}{8} & \frac{1}{8} & \frac{1}{8} & \frac{1}{8} & 0 & 0 & 0 & 0 & -\frac{1}{8} & -\frac{1}{8} & -\frac{1}{8} & -\frac{1}{8} \\ \frac{1}{12} & -\frac{1}{12} & -\frac{1}{12} & \frac{1}{12} & \frac{1}{12} & -\frac{1}{12} & -\frac{1}{12} & \frac{1}{12} & \frac{1}{12} & -\frac{1}{12} & -\frac{1}{12} & \frac{1}{12} \\ \frac{1}{8} & \frac{1}{8} & \frac{1}{8} & \frac{1}{8} & -\frac{1}{4} & -\frac{1}{4} & -\frac{1}{4} & -\frac{1}{4} & \frac{1}{8} & \frac{1}{8} & \frac{1}{8} & \frac{1}{8} \\ -\frac{3}{20} & -\frac{1}{20} & \frac{1}{20} & \frac{3}{20} & 0 & 0 & 0 & 0 & \frac{3}{20} & \frac{1}{20} & -\frac{1}{20} & -\frac{3}{20} \end{bmatrix}. \tag{52}$$

Figures 16 through 21 compare the results of compatibility tests between frames BILD10 and BILD11 as well as between BILD11 and BILD12 depicted in Fig. 1 for the constant, linear, and quadratic picture function models according to Eqs. (13),

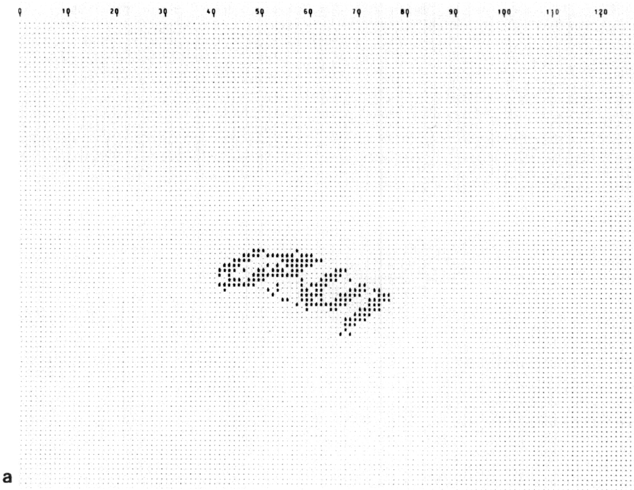

a

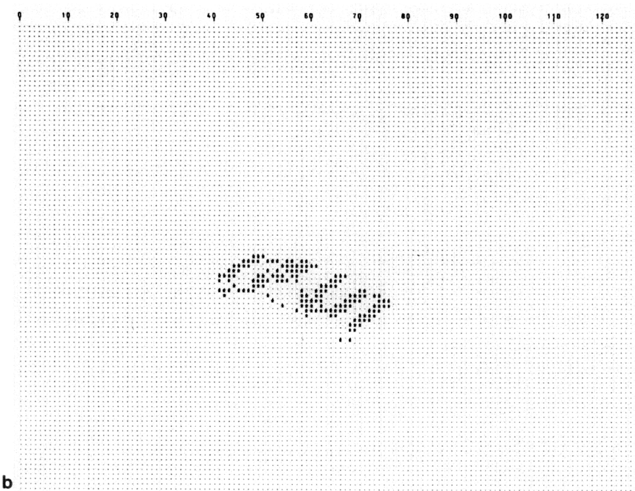

b

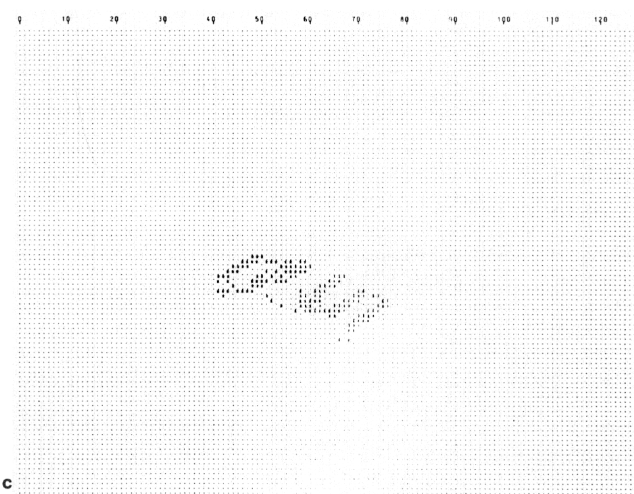

c

FIG. 16. Results of compatibility tests between frames BILD10 and BILD11 for the constant picture function model according to Eq. (13). The confidence level has been chosen as (a) $\alpha = 0.05$, $T = 2.948$; (b) $\alpha = 0.01$, $T = 6.29$; (c) $\alpha = 0.005$, $T = 7.95$.

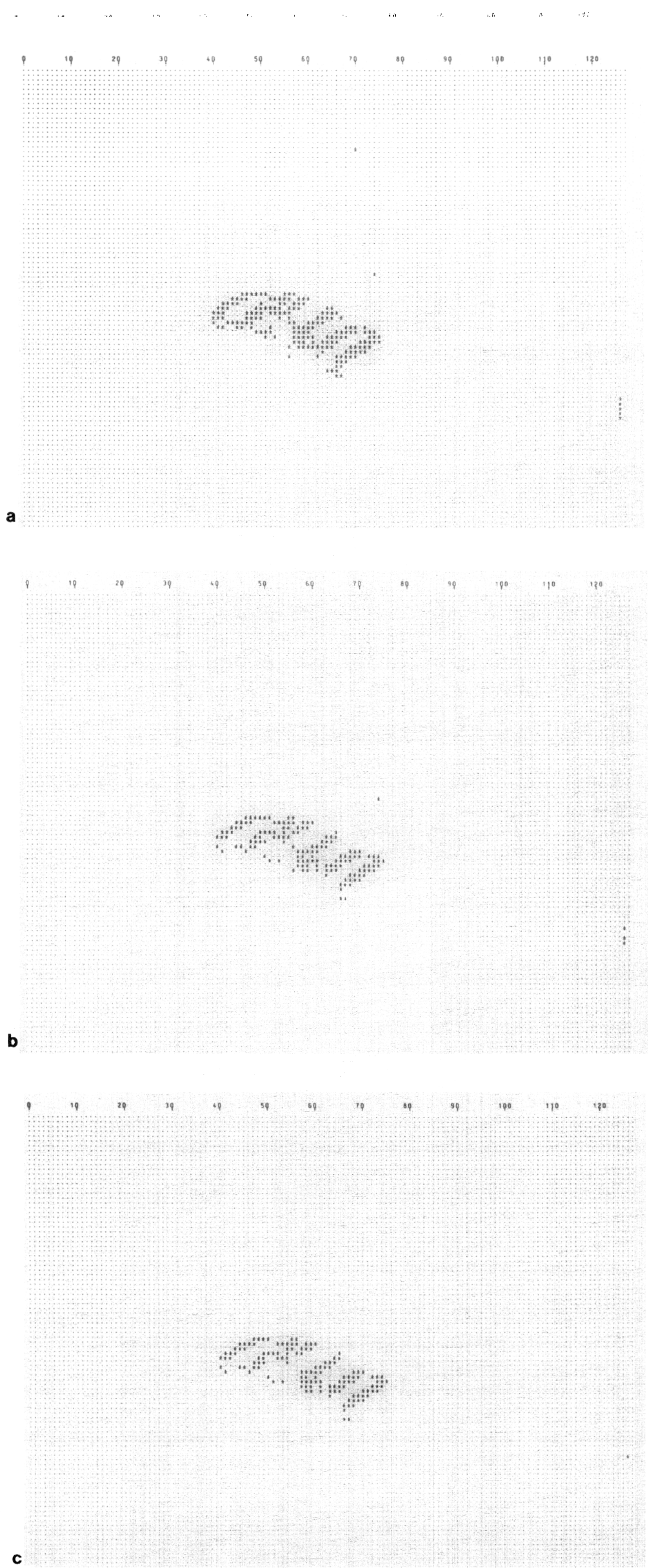

FIG. 17. Analogous results of compatibility tests between frames BILD11 and BILD12: (a) $\alpha = 0.05$, $T = 2.948$; (b) $\alpha = 0.01$, $T = 6.29$; (c) $\alpha = 0.005$, $T = 7.95$.

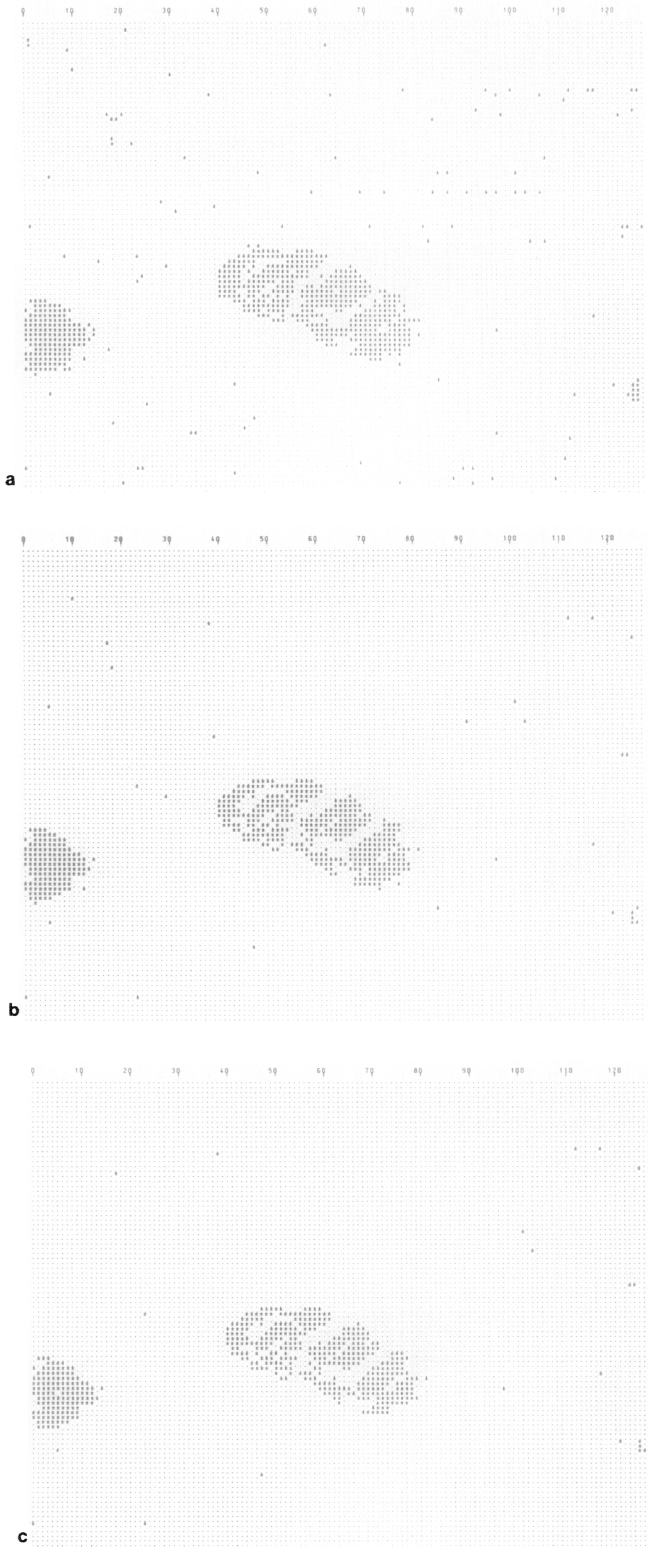

FIG. 18. Results of compatibility tests between BILD10 and BILD11 using the linear picture function model according to Eq. (28): (a) $\alpha = 0.05$, $F = 3.16$; (b) $\alpha = 0.01$, $F = 5.14$; (c) $\alpha = 0.005$, $F = 6.08$.

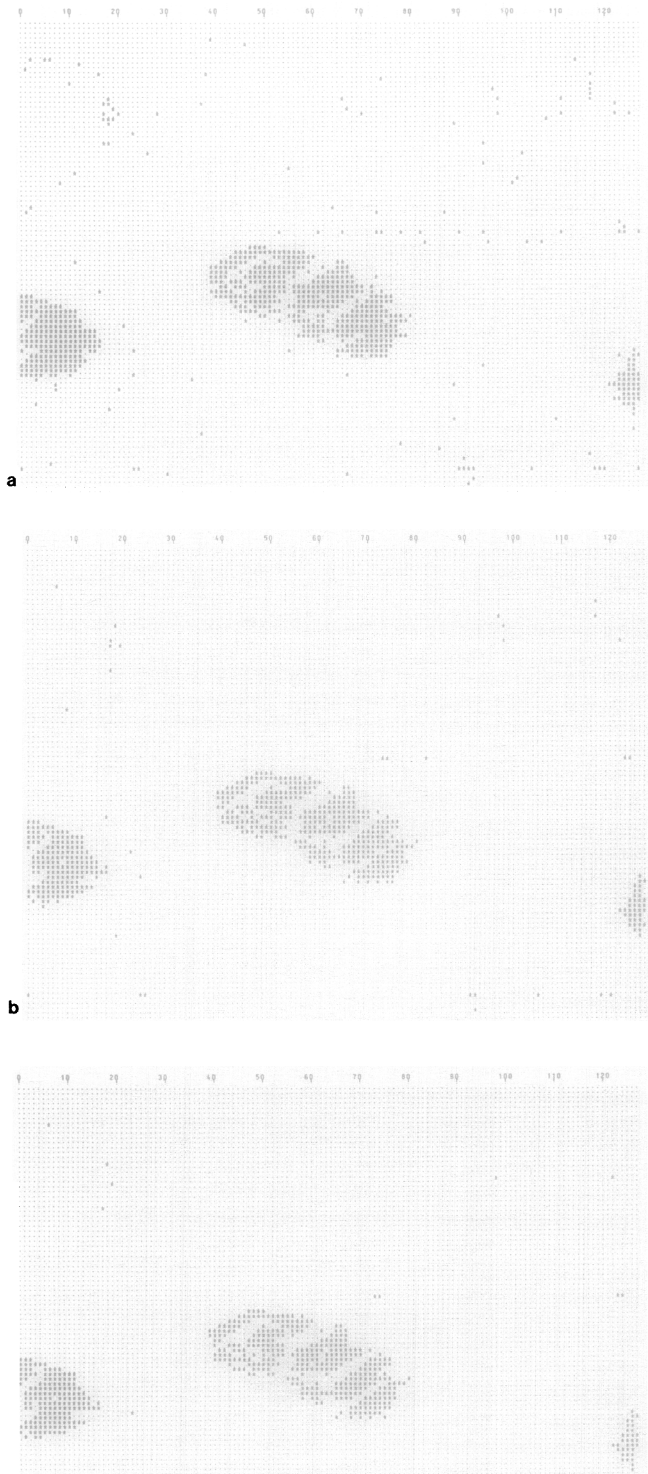

FIG. 19. Analogous to Fig. 18, but comparing BILD11 and BILD12: (a) $\alpha = 0.05$, $F = 3.16$; (b) $\alpha = 0.01$, $F = 5.14$; (c) $\alpha = 0.005$, $F = 6.08$.

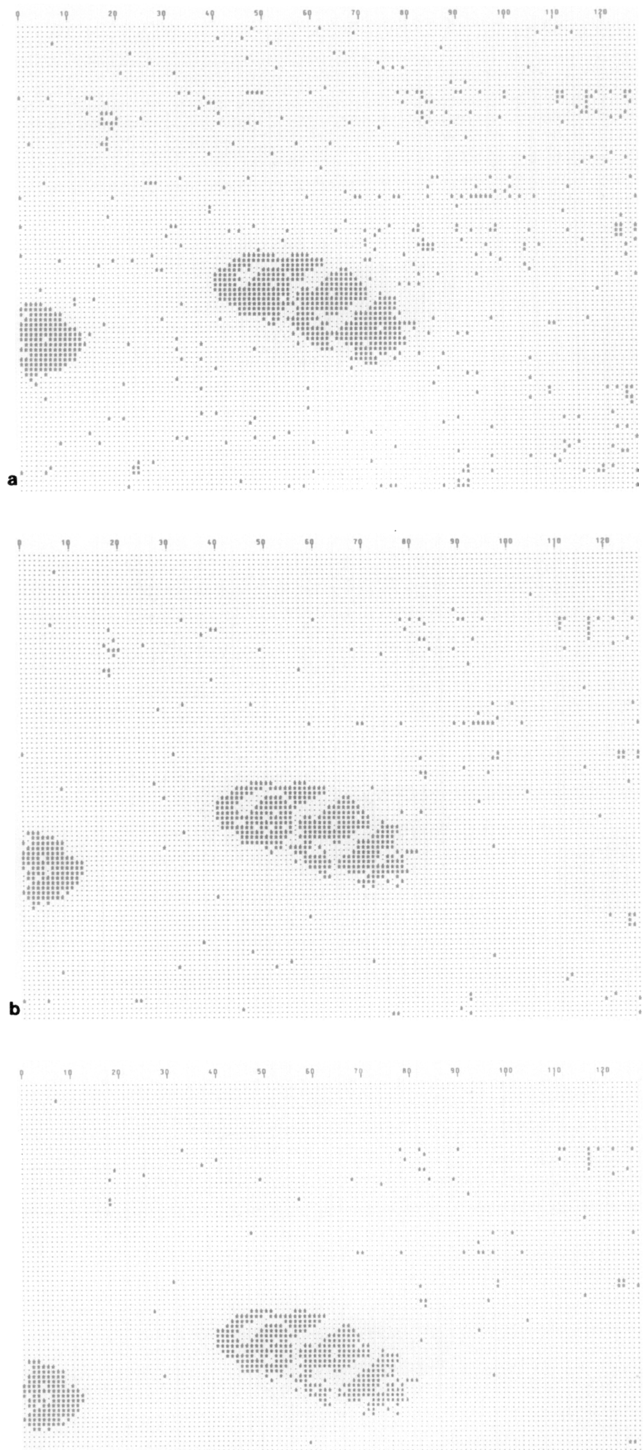

FIG. 20. Results of compatibility tests based on the quadratic picture function model according to Eq. (49) for BILD10 and BILD11: (a) $\alpha = 0.05$, $F = 3.00$; (b) $\alpha = 0.01$, $F = 4.82$; (c) $\alpha = 0.005$, $F = 5.76$.

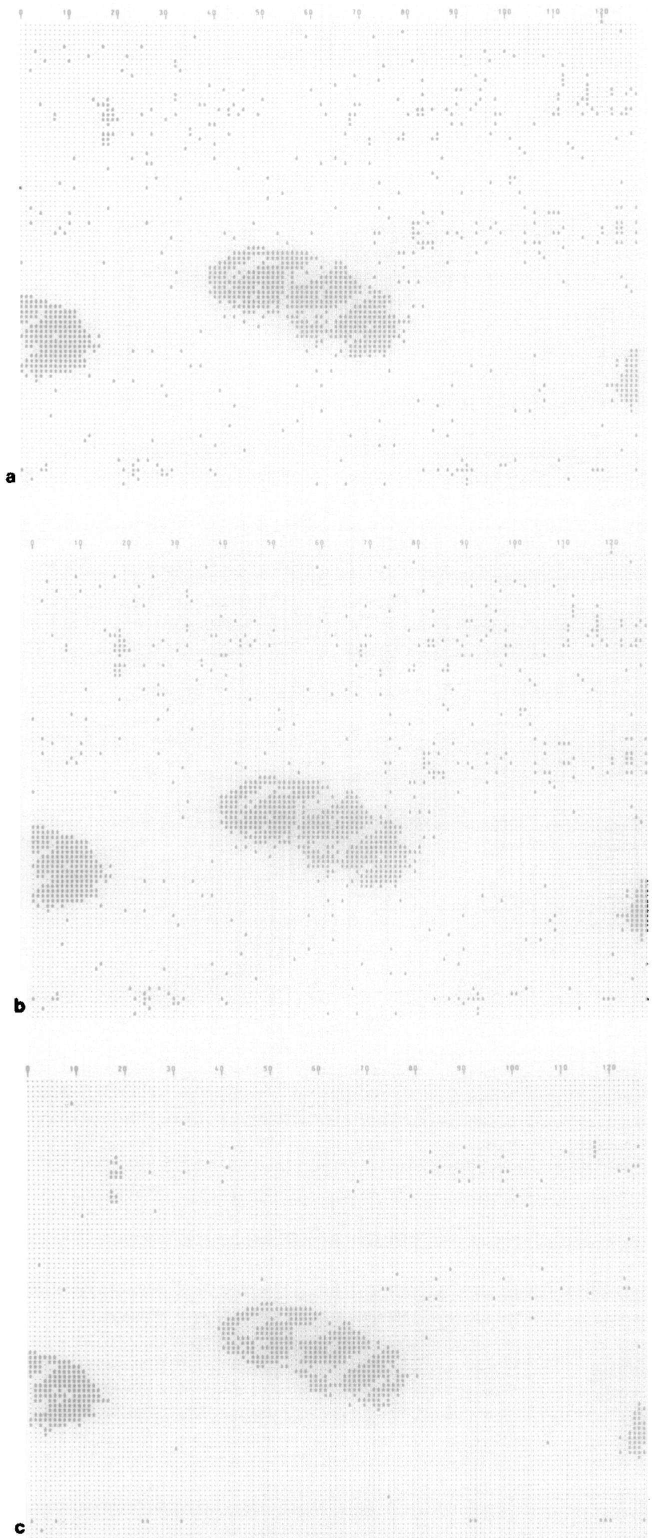

FIG. 21. Analogous to Fig. 20, but comparing BILD11 and BILD12: (a) $\alpha = 0.05$, $F = 3.00$; (b) $\alpha = 0.01$, $F = 4.82$; (c) $\alpha = 0.005$, $F = 5.76$.

(28), and (49), respectively. Three different confidence levels have been chosen, for example, $\alpha = 0.005$; i.e., the probability is only 0.5% that corresponding test areas from these two half-frames have been marked by an asterisk as being incompatible although the original images projected onto the target of the TV camera did not change. Only the accumulation of random errors caused the associated likelihood ratio to exceed the threshold specified by the chosen confidence level. It is obvious that the compatibility test becomes more sensitive as we improve the picture function model from a constant gray-value distribution to a quadratic dependence of gray values on the pixel coordinates.

Figures 18 through 21 present results for tests based on linear and quadratic picture function models with different values of $\alpha = 0.05$, $\alpha = 0.01$, and $\alpha = 0.005$, i.e., increasing confidence that test areas marked as being incompatible are indeed due to image changes rather than to statistical fluctuations in the digitized data. For the combination of images and test area size employed in these experiments, the transition from a linear to a quadratic picture function does not produce as striking an improvement as the transition between constant and linear picture functions; compare Figs. 16 and 18. Nevertheless, the use of a quadratic picture function increases our confidence in the compatibility test decisions although it does not seem necessary to use an even more complex third-order picture function model.

Comparison with the results of the likelihood test according to Eq. (2) or (3)—the latter combined with Eq. (4) or (5) for a linear or quadratic picture function—shows that the statistical tests (13), (28), and (49) derived upon the assumption of common variance for both test areas facilitate a more sensitive discrimination between compatible and truly incompatible areas. For a given model of the picture function in the test area, the statistical tests derived in Sections 5 through 7 yield about the same sensitivity as the ones discussed in Sections 2 through 4—but at a lower threshold value. In other words, the tests derived in Sections 5 through 7 yield the same sensitivity with higher confidence. These results, therefore, support the assumption that the variance of sampled gray values computed on the basis of a quadratic picture function model is indeed due to random noise. This observation justifies the selection of decision thresholds based on a priori confidence limits rather than interactive adjustment for each individual image sequence.

ACKNOWLEDGMENTS

We thank L. Dreschler, G. Hille, and B. Neumann for many discussions, and especially L. Dreschler for providing Figs. 1 and 11. The first author (Y. Z. Hsu) gratefully acknowledges discussions and helpful suggestions by Mr. Zhou. We are grateful to Mrs. R. Jancke for her help in typing this manuscript.

REFERENCES

1. L. Dreschler, Ermittlung markanter Punkte auf den Bildern bewegter Objekte und Berechnung einer 3D-Beschreibung auf dieser Grundlage, Dissertation, Fachbereich Informatik, Universität Hamburg, June 1981.
2. L. Dreschler and H.-H. Nagel, Volumetric model and 3D-trajectory of a moving car derived from monocular TV-frame sequences of a street scene, IJCAI-81, pp. 692–697. *Comput. Graphics Image Processing* **20**, 1982, 199–228.
3. L. Dreschler and H.-H. Nagel, On the selection of critical points and local curvature extrema of region boundaries for interframe matching, Fachbereich Informatik, Universität Hamburg, Feb. 1982. ICPR-82, pp. 542–544.

4. R. M. Haralick, Edge and region analysis for digital image data, *Comput. Graphics Image Processing* **12**, 1980, 60–73.
5. R. M. Haralick and L. Watson, A facet model for image data, IEEE Conference on Pattern Recognition and Image Processing, 1979, pp. 489–497; *Comput. Graphics Image Processing* **15**, 1981, 113–129.
6. F. Holdermann and H. Kazmierczak, Preprocessing of gray-scale pictures, *Comput. Graphics Image Processing* **1**, 1972, 66–80.
7. T. S. Huang (Ed.), *Image Sequence Analysis*, Springer-Verlag, Berlin–Heidelberg–New York, 1981.
8. R. Jain, Dynamic scene analysis using pixel-based processes, *IEEE Comput.* **14**, No. 8, Aug. 1981, 12–17.
9. R. Jain and H.-H. Nagel, On the analysis of accumulative difference pictures from image sequences of real world scenes, *IEEE Trans. Pattern Anal. Mach. Intell.* **PAMI-1**, 1979, 206–214.
10. R. Jain, D. Militzer and H.-H. Nagel, Separating non-stationary from stationary scene components in a sequence of real world TV-images, IJCAI-77, pp. 612–618.
11. R. Jain, W. N. Martin, and J. K. Aggarwal, Segmentation through the detection of changes due to motion, *Comput. Graphics Image Processing* **11**, 1979, 13–34.
12. D. Militzer, Erkennen nicht-stationaerer Bildkomponenten in Folgen von TV-Aufnahmen, Diplomarbeit, Fachbereich Informatik, Universität Hamburg, November 1977 (unpublished).
13. H.-H. Nagel, Experiences with Yakimovsky's algorithm for boundary and object detection in real world images, IJCPR-76, pp. 753–758.
14. H.-H. Nagel, Formation of an object concept by analysis of systematic time variations in the optically perceptible environment, *Comput. Graphics Image Processing* **7**, 1978, 149–194.
15. H.-H. Nagel, Recent advances in motion interpretation based on image sequences, Proc. IEEE International Conference on Acoustics, Speech and Signal Processing, Paris, May 3–5, 1982, pp. 1179–1186.
16. H.-H. Nagel, Displacement vectors derived from second order intensity variations in image sequences, FBI-HH/M-97/82, March 1982, Fachbereich Informatik, Universität Hamburg. *Comput. Graphics Image Processing* **21** (1983), 85–117.
17. H.-H. Nagel and W. Enkelmann, Investigation of second order grey-value variations to estimate corner point displacements, Fachbereich Informatik, Universität Hamburg, January 1982. ICPR-82, pp. 768–773.
18. H.-H. Nagel and G. Rekers, Moving object masks based on an improved likelihood test, Fachbereich Informatik, Universität Hamburg, Feb. 1982. ICPR-82, pp. 1140–1142.
19. T. C. Pong, L. G. Shapiro, and R. M. Haralick, A facet model region growing algorithm, *IEEE Conf. Pattern Recognition Image Processing*, 1981, pp. 279–284.
20. B. Radig, Description of moving objects based on parameterized region extraction, IJCPR-78, pp. 723–725.
21. B. M. Radig, Image region extraction of moving objects, in *Image Sequence Analysis* (T. S. Huang, Ed.), pp. 311–354, Springer-Verlag, Berlin–Heidelberg–New York, 1981.
22. G. Rekers, Die Charakterisierung von Zustaenden und Zustandsaenderungen in Strassenszenen sowie deren Identifizierung in TV-Bildfolgen, Diplomarbeit, Fachbereich Informatik, Universität Hamburg, Feb. 1982.
23. Y. Yakimovsky, Boundary and object detection in real world images, *J. ACM* **23**, 1976, 599–618.